

NIST Series Technical Note  
2185

Thermal and gas mixture  
composition measurements  
preceding backdrafts in a 2/5<sup>th</sup>  
scale compartment

Ryan Falkenstein-Smith  
Thomas Cleary

This publication is available free of charge from:  
<https://doi.org/10.6028/NIST.TN.2185>

NIST Series Technical Note  
2185

Thermal and gas mixture  
composition measurements  
preceding backdrafts in a 2/5<sup>th</sup>  
scale compartment

Ryan Falkenstein-Smith  
Thomas Cleary  
*Fire Research Division  
Engineering Laboratory*

This publication is available free of charge from:  
<https://doi.org/10.6028/NIST.TN.2185>

September 2022



U.S. Department of Commerce  
*Gina M. Raimondo, Secretary*

National Institute of Standards and Technology  
*Laurie E. Locascio, NIST Director and Under Secretary of Commerce for Standards and Technology*

Certain commercial entities, equipment, or materials may be identified in this document in order to describe an experimental procedure or concept adequately. Such identification is not intended to imply recommendation or endorsement by the National Institute of Standards and Technology, nor is it intended to imply that the entities, materials, or equipment are necessarily the best available for the purpose.

#### **NIST Technical Series Policies**

[Copyright, Fair Use, and Licensing Statements](#)

[NIST Technical Series Publication Identifier Syntax](#)

#### **How to cite this NIST Technical Series Publication:**

Ryan Falkenstein-Smith, Thomas Cleary ( 2022) Thermal and gas mixture composition measurements preceding backdrafts in a 2/5<sup>th</sup> scale compartment. (National Institute of Standards and Technology, Gaithersburg, MD), 2185. <https://doi.org/10.6028/NIST.TN.2185>

#### **NIST Author ORCID iDs**

Ryan Falkenstein-Smith: 0000-0001-7039-5835

Thomas Cleary: 0000-0001-8785-2035

#### **Contact Information**

[ryan.falkenstein-smith@nist.gov](mailto:ryan.falkenstein-smith@nist.gov)

## **Abstract**

This report documents real-time and time-averaged temperature, global and local equivalence ratios, and oxygen, carbon dioxide, and carbon monoxide concentration measurements made at various positions in an isolated 2/5<sup>th</sup> scale compartment prior to a backdraft event. The compartment was subjected to methane, propane, and propylene fires of different sizes and fuel flow times. Backdrafts were observed to vary depending on the fuel source. Gas mixture composition measurements obtained before an anticipated backdraft were obtained through various gas analysis techniques, including an enhanced phi meter, a gas analyzer equipped with one paramagnetic and two non-dispersive infrared sensors, and a Gas Chromatograph/Mass Spectrometer System. Measurements and the influence of transient compartment conditions, including opening configuration, spark igniter location, fire size, and fuel flow time, are discussed in detail. The likelihood of backdraft under these compartment configurations is typically improved with a higher spark igniter location and fire size, smaller compartment opening, and shorter fuel flow time.

## **Key words**

Backdraft; Gas Species Concentrations; Global Equivalence Ratio; Local Equivalence Ratio; Reduced-Scale Enclosure; Real-time Measurements; Time-averaged Measurements.

## Table of Contents

1. Introduction . . . . .	1
2. Description of Experiments . . . . .	1
2.1. Compartment configuration . . . . .	1
2.2. Experimental procedure . . . . .	2
2.3. Gas composition measurements . . . . .	4
3. Results . . . . .	6
3.1. Temperature measurements . . . . .	6
3.1.1. Real-Time temperature measurements . . . . .	6
3.1.2. Time-Averaged temperature measurements . . . . .	10
3.2. Gas mixture composition measurements . . . . .	14
3.2.1. Real-Time gas mixture composition measurements . . . . .	14
3.2.2. Time-Averaged gas mixture composition measurements . . . . .	21
4. Verifying Gas Composition Measurements . . . . .	29
5. Probabilities of Backdraft at varying experimental conditions . . . . .	31
6. Conclusion . . . . .	39
References . . . . .	40
Appendix A. Uncertainty Analysis of Real-time Measurements . . . . .	42
A.1. Temperature . . . . .	42
A.2. Gas Species Concentration Measurements obtained via Gas Analyzer . . . . .	42
A.3. Global Equivalence Ratio . . . . .	42
A.4. Local Equivalence Ratio . . . . .	43
Appendix B. Uncertainty Analysis of Time-Averaged Measurements . . . . .	44

## List of Tables

Table 1. List of fuel flow times for each fire configuration . . . . .	4
Table 2. List of uncertainties for gas analyzer components. . . . .	42
Table 3. List of uncertainties for selected phi meter components. . . . .	43

## List of Figures

Fig. 1. Schematic of the 2/5 <sup>th</sup> scale compartment utilized for backdraft experiments. . . . .	3
--	---

Fig. 2.	Real-time temperature measurements of the 25.0 kW, 31.3 kW, and 37.5 kW methane fires within the compartment prior to backdraft . . . . .	7
Fig. 3.	Real-time temperature measurements of the 16.7 kW, 20.9 kW, and 25.0 kW propane fires within the compartment prior to backdraft . . . . .	8
Fig. 4.	Real-time temperature measurements of a 25.0 kW propylene fire within the compartment prior to backdraft . . . . .	9
Fig. 5.	Time-averaged temperature measurements of the 25.0 kW, 31.3 kW, and 37.5 kW methane fires within the compartment prior to backdraft . . . . .	11
Fig. 6.	Time-averaged temperature measurements of the 16.7 kW, 20.9 kW, and 25.0 kW propane fires within the compartment prior to backdraft . . . . .	12
Fig. 7.	Time-averaged temperature measurements of the 25.0 kW propylene fire within the compartment prior to backdraft . . . . .	13
Fig. 8.	Real-time gas mixture composition measurements of the 25.0 kW, 31.3 kW, and 37.5 kW methane fires within the compartment prior to backdraft . . . . .	17
Fig. 9.	Sequences of flame propagation in the compartment previously subjected to 25.0 kW methane, propane, and propylene fires with a fuel flow time of 450 s, 300 s, 270 s, respectively. . . . .	18
Fig. 10.	Real-time gas mixture composition measurements of the 16.7 kW, 20.9 kW, and 25.0 kW propane fires within the compartment prior to backdraft . . . . .	19
Fig. 11.	Real-time gas mixture composition measurements of a 25.0 kW propylene fire within the compartment prior to backdraft . . . . .	20
Fig. 12.	Time-averaged gas mixture composition measurements of the 25.0 kW, 31.3 kW, and 37.5 kW methane fires within the compartment prior to backdraft . . . . .	22
Fig. 13.	Time-averaged gas mixture composition measurements of the 16.7 kW, 20.9 kW, and 25.0 kW propane fires within the compartment prior to backdraft . . . . .	23
Fig. 14.	Time-averaged gas mixture composition measurements of the 25.0 kW propylene fire within the compartment prior to backdraft . . . . .	24
Fig. 15.	Time-averaged gas species concentration measurements obtained via GC/MSD of the 25.0 kW, 31.3 kW, and 37.5 kW methane fires within the compartment prior to backdraft . . . . .	26
Fig. 16.	Time-averaged gas species concentration measurements obtained via GC/MSD of the 16.7 kW, 20.9 kW, and 25.0 kW propane fires within the compartment prior to backdraft . . . . .	27
Fig. 17.	Time-averaged gas species concentration measurements obtained via GC/MSD of the 25.0 kW propylene fires within the compartment prior to backdraft . . . . .	28
Fig. 18.	Time-averaged gas mixture composition measurements obtained via phi meter and gas analyzers compared against time-averaged measurements made via GC/MSD . . . . .	30
Fig. 19.	Conditional density plot of a 25 kW methane fire as a function of fuel flow time at various compartment configurations . . . . .	32
Fig. 20.	Conditional density plot of a 31.3 kW methane fire as a function of fuel flow time at various compartment configurations . . . . .	33

Fig. 21. Conditional density plot of a 37.5 kW methane fire as a function of fuel flow time at various compartment configurations . . . . .	34
Fig. 22. Conditional density plot of a 16.7 kW propane fire as a function of fuel flow time at various compartment configurations . . . . .	35
Fig. 23. Conditional density plot of a 20.9 kW propane fire as a function of fuel flow time at various compartment configurations . . . . .	36
Fig. 24. Conditional density plot of a 25.0 kW propane fire as a function of fuel flow time at various compartment configurations . . . . .	37
Fig. 25. Conditional density plot of a 25.0 kW propylene fire as a function of fuel flow time at various compartment configurations . . . . .	38

## **Acknowledgments**

The authors would like to acknowledge Christopher Brown, Marcos Fernandez, Laurean DeLauter, and Michael Selepak, who aided in the collection of the experimental datasets.

## 1. Introduction

Backdrafts are a severe fire phenomenon that poses a life-threatening risk to anyone who may encounter them. A backdraft occurs in an isolated heated enclosure starved of oxygen with a substantial concentration of unburned fuel. When an opening is suddenly introduced in the enclosure, a gravity current of colder air is driven inward, mixing with the residing heated fuel. In the presence of an ignition source, a localized flammable mixture can ignite, deflagrate, and generate an extending flame and pressure wave through the enclosure's opening.

Fleishmann et al. [1] established the physical mechanisms conducive to a backdraft phenomenon, such as the gravity current generated at the opening, turbulent mixing within the enclosure, and ignition. Refs. [2–12] have expanded upon understanding the backdraft phenomenon by examining the correlation between backdraft intensity and fuel type, compartment size, and vent/opening configurations. In order to resolve the subtle impact of the gravity current, gas mixing, ignition, and flame propagation, some works [13–17] have relied on computational fluid dynamics (CFD) models. The primary objective of this work is to provide a comprehensive dataset that better informs CFD models about physical and chemical properties within an enclosure preceding a potential backdraft.

This report characterizes the spatial distribution of temperature and gas mixture compositions from an experimental campaign focused on studying backdraft in a 2/5<sup>th</sup> scale compartment. Equivalence ratios and gas species measurements are recorded at various positions within the compartment, a portion surrounding a controlled ignition source. Here, methane, propane, and propylene are the fuels of interest. Temperature measurements recorded throughout the compartment are also provided.

## 2. Description of Experiments

All experiments were conducted at the National Fire Research Laboratory under a 3 MW calorimeter (6 m canopy hood) [18]. Total heat release measurements conducted in the canopy hood via oxygen consumption calorimetry are provided in Ref. [19]. All experimental conditions described in this work were repeated at least twice.

### 2.1. Compartment configuration

All backdraft experiments were conducted in a reduced-scale enclosure (1.0 m x 1.0 m x 1.5 m), 2/5<sup>th</sup> the dimensions of the ASTM fire test room. The enclosure's front had a pneumatically operated door along a short wall with a 43.0 cm wide and 80.0 cm high opening. The door opening is transformed into a window configuration by adding a 15.2 cm high lip to the front entryway, forming a sill covering the lower half of the opening. Figure 1 provides a schematic of the compartment with the spark igniters, gas sampling probes, and thermocouples positions. In this experimental series, two spark igniter positions were used

in either the middle or low spark position, 25.4 cm or 50.7 cm from the compartment floor, respectively. Gas species measurements were obtained in the center of the compartment (50.0 cm from the sidewall) using a stainless steel gas sampling line positioned at varying heights from the compartment floor ranging from 90.0 cm to 22.0 cm, and lateral positions spanning 37.5 cm and 111.0 cm from the opening of the compartment.

Temperature measurements were obtained from two thermocouple arrays on opposing sides of the compartment. The first thermocouple array used 49.5 cm long Type K thermocouples configured in a rectangular orientation on the left wall facing the door. The second thermocouple array comprised of four 24.8 cm long Type K thermocouples configured in a line on the right wall facing the door spaced approximately 19.9 cm apart. All temperature measurements were sampled at 1.0 Hz using a data acquisition system (DAQ) for most of the experiment except for a 60 s time-interval, 20 s prior, and 40 s after an anticipated backdraft, in which the sampling rate increased to 25.0 Hz. The uncertainty analysis for temperature measurements is described in Appendix A.1.

Gaseous fuels were fed into a 17.8 cm square sand burner whose center was approximately 1.25 m from the front opening of the compartment. In some instances, a boroscope was implemented to observe the flame structure at the burner while the compartment remained closed. A 3.8 cm diameter vent was constructed in the lower right wall of the compartment, 38.0 cm from the front interior wall of the compartment, and 3.0 cm above the compartment floor. The vent's purpose was to prevent overpressure within the compartment by allowing a uniform leakage area when the door is closed. A detailed description of the compartment is available in Ref. [20].

## 2.2. Experimental procedure

Backdraft experiments were initiated when a small sand burner, fed fuel via mass flow controller, was ignited using a propane wand ( $t=0$ ). Initially, the fire burned while the compartment doorway remained open for 60 s ( $t=60$ ). After the front doorway was closed, fuel continued to be fed into the sand burner until a predetermined fuel flow time was achieved ( $t=\text{fuel flow time}$ ). The doorway remained closed for an additional 30 s, after which the doorway opened, and a potential backdraft was observed ( $t=\text{fuel flow time}+30$ ).

Backdraft measurements were obtained using either methane, propane, or propylene as a fuel source. Methane fire sizes included 25.0 kW, 31.3 kW, and 37.5 kW. Propane fire sizes included 16.7 kW, 20.9 kW, and 25.0 kW. Propylene fire sizes only include 25.0 kW. Fuel flow times were adjusted following fire size. A list of fuel flow times for each fire configuration is provided in Table 1. The uncertainty for all fire sizes was approximately 1.0 kW.



**Table 1.** List of fuel flow times for each fire configuration

Fuel	Fire size (kW)	Fuel flow time (s)
Methane	25.0 ± 1.0 kW	360, 390, 420, 450
	31.3 ± 1.0 kW	300, 360
	37.5 ± 1.0 kW	240, 270, 285, 300
Propane	16.7 ± 1.0 kW	270, 300, 315, 330
	20.9 ± 1.0 kW	210, 225, 240, 285
	25.0 ± 1.0 kW	240, 270, 285, 300
Propylene	25.0 ± 1.0 kW	210, 240, 270

### 2.3. Gas composition measurements

Measurements of gas mixture compositions were examined at two locations within the compartment for each backdraft experiment. Each sampling position was located approximately 50.0 cm ± 2.0 cm from the sidewall of the compartment. In total, three sets of different locations were selected as positions of interest:

1. In the upper (y=94.0 cm) and middle (y=49.5 cm) layer of the compartment towards the front (x=37.5 cm)
2. Approximately 5.0 cm above (y=56.0 cm) and below (y=46.0 cm) the middle spark igniter (y=50.7 cm) in the back of the compartment (x=111.0 cm)
3. Approximately 7.0 cm above (y=32.5 cm) and 3.0 cm below (y=22.0 cm) the low spark igniter (y=25.4 cm) in the back of the compartment (x=111.0 cm)

In experiments where gas samples were extracted around a spark igniter, the igniter of interest was the only source of ignition.

Extracted gas samples were portioned into a gas analyzer, a 300 ml stainless steel reservoir fitted with baffles, and a phi meter at all locations. The gas analyzer included one paramagnetic and two non-dispersive infrared sensors to provide real-time oxygen, O<sub>2</sub>, carbon dioxide, CO<sub>2</sub>, and carbon monoxide, CO, concentration measurements. A chiller fitted with a large volume particulate filter at its inlet was positioned upstream of the gas analyzer to prevent water vapor and soot from compromising the analyzer. The presence of the chiller indicates that all O<sub>2</sub>, CO<sub>2</sub>, and CO concentration measurements were obtained on a dry basis. A description of the uncertainty analysis for O<sub>2</sub>, CO<sub>2</sub>, and CO concentration measurements obtained from the gas analyzer is described in Appendix A.2.

The stainless-steel reservoir was used to collect well-mixed gas samples that an Agilent 5977E Series Gas Chromatograph analyzed with thermal conductivity and mass selectivity detectors (GC/MSD). The GC/MSD analysis provided time-averaged gas species concentrations of combustion products using a method described in Refs. [21, 22]. Gas samples were extracted through a sampling line via a vacuum pump for 1 min, initiated 70 s before the door opened (t=fuel flow time-40). Time-averaged species concentration measure-

ments were estimated to represent an extracted gas mixture obtained 20 s before the door opening. A detailed description of the uncertainty analysis of time-averaged gas species measurements obtained via GC/MSD is reported in Ref. [21].

A phi meter [23, 24] was implemented to evaluate the extracted gas sample's global and local equivalence ratios. Unlike other gas sampling techniques [25, 26], a phi meter provides real-time equivalence ratio measurements without knowledge of the initial fuel or combusted gas mixture. The phi meter utilizes a high-temperature catalytic reactor to facilitate lean combustion via excess oxygen to the sampling line. The lean combustion results in an exhaust exclusively comprised of oxygen, carbon dioxide, water vapor, and inert gases. The reactor exhaust is then cooled to condense water from the gas line preserving the integrity of downstream measurement devices. Downstream measurement devices include a mass flow controller, vacuum pump, and gas analyzer capable of measuring oxygen and carbon dioxide concentrations. The mass flow controller is implemented to regulate the total flow through the phi meter's reactor, driven by the downstream vacuum pump. Before entering the pump, oxygen and carbon dioxide concentration measurements of the gas stream are recorded and used to calculate the global equivalence ratio.

The global equivalence ratio,  $\phi_G$ , is calculated by the phi meter's  $O_2$  and  $CO_2$  concentration measurements in the dried reactor's exhaust stream,  $X_{O_2}$  and  $X_{CO_2}$ , and the mass flow controller volumetric flow,  $\dot{V}_{MFC}$ , measurements in the equation below, where  $X_{O_2,Ent}$  is the concentration of oxygen in the air (approx. 20.95%) and  $\dot{V}_{O_2,Ex}$  is the volumetric flows of the excess oxygen, respectively.

$$\phi_G = 1 + \left( \frac{1 - X_{O_2,Ent}}{X_{O_2,Ent}(1 - X_{O_2} - X_{CO_2})} \right) \left( \frac{\dot{V}_{O_2,Ex}}{\dot{V}_{MFC}} - X_{O_2,A} \right) \quad (1)$$

The local equivalence ratio,  $\phi_L$ , is estimated from the phi meter by determining the oxygen consumption for the lean combustion in the reactor, as defined in the equation below.

$$\phi_L = 1 + \frac{\dot{m}_{O_2,Ex.} - \dot{m}_{O_2,O}}{\dot{m}_{O_2,Samp.}} \quad (2)$$

Here,  $\dot{m}_{O_2,Ex.}$  is the mass flow of excess oxygen introduced at the inlet of the phi meter,  $\dot{m}_{O_2,O}$  is the mass flow of oxygen measured at the outlet of the phi meter's reactor, and  $\dot{m}_{O_2,Samp.}$  is the mass flow of oxygen in the extracted sample at the inlet of the phi meter. The oxygen concentration in the extracted sample is estimated from  $O_2$  measurements provided by the external paramagnetic sensor. A full derivation of Eq. 2 is provided in Ref. [24]. Uncertainty analyses of the phi meter's global and local equivalence ratio measurements is given in Appendix A.3 and A.4, respectively.

Sample lines feeding into the phi meter and stainless-steel reservoir were heated to approximately  $90 \text{ }^\circ\text{C} \pm 5 \text{ }^\circ\text{C}$  using heating tape, which prevented water vapor condensation in the extracted sample. Gas species concentrations in the paramagnetic sensor and phi meter data were recorded at 1 Hz throughout the experiment using a DAQ.

### 3. Results

This section presents real-time and averaged temperature and gas mixture composition measurements taken at different positions within the enclosure before an anticipated backdraft.

#### 3.1. Temperature measurements

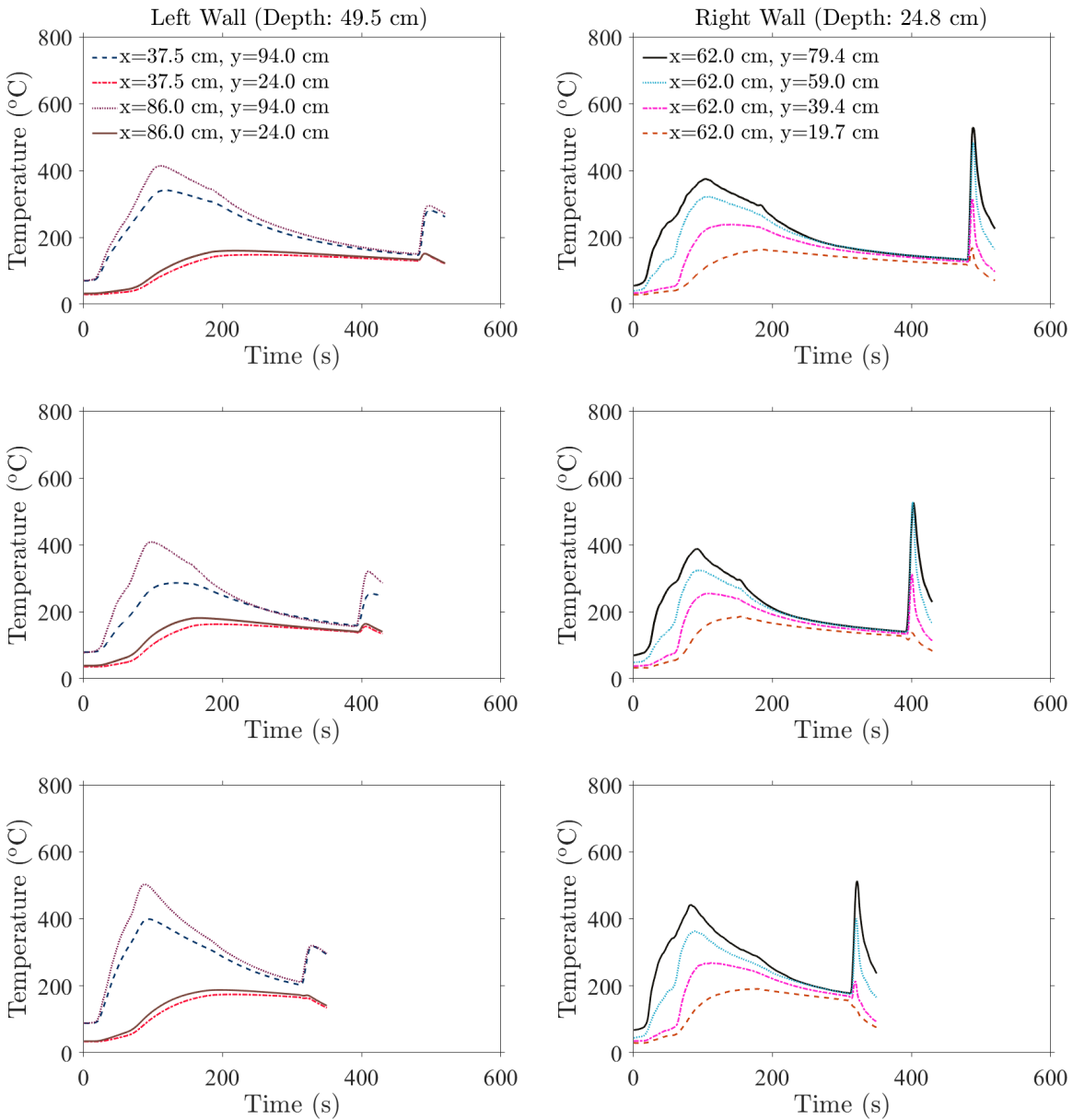
##### 3.1.1. Real-Time temperature measurements

Figure 2 presents the real-time temperature measurements from both thermocouple arrays of the 25.0 kW, 31.3 kW, and 37.5 kW methane fires subjected to different fuel flow times. The temperature steadily increased for each methane fire configuration until the flame was extinguished, causing the temperature to peak and then decline. The extinguished flame was confirmed via boroscope observation. When a backdraft occurs, temperatures at all positions within the compartment spike, then rapidly decline. No spike was observed in instances where a backdraft did not occur, and the temperature declined steadily.

The temperature data measured on the left wall of the enclosure demonstrates that temperatures were higher in the upper region and back of the compartment, farther away from the doorway and vent. The right wall temperature profiles further demonstrate the temperature gradient as a function of height, wherein temperatures were higher farther up within the compartment. The initial temperature climb before the flame diminishing is observed to increase faster with fire size at most positions within the enclosure.

Experiments utilizing propane fires are shown to echo similar temperature profiles as that of experiments with methane fires and are displayed in Fig. 3. Here, real-time temperature measurements from both thermocouple arrays of the 16.7 kW, 20.9 kW, and 25.0 kW propane fires subjected to different fuel flow times are shown. Temperatures were higher at locations farther up and back within the compartment. Initial temperature ramps and peaks are shown to increase with propane fire size. Compared to an experiment utilizing a 25.0 kW methane fire, the 25.0 kW propane fire size demonstrates higher temperature profiles at most positions.

Figure 4 displays the temperature profiles obtained from both thermocouple arrays for a 25.0 kW propylene fire with a fuel flow time of 270 s. Similar temperature profiles are exhibited. Compared to the temperature profiles in experiments with a 25.0 kW propane fire size, the initial peak temperature is lower and less distinguishable on the left wall.



**Fig. 2.** Real-time temperature measurements of the 25.0 kW methane fire with a fuel flow time of 450 s (top), the 31.3 kW methane fire with a fuel flow time of 360 s (middle), and the 37.5 kW methane fire with a fuel flow time of 285 s (bottom) at different positions within the compartment. The expanded uncertainty of the temperature measurement estimated from the Type B evaluation of standard uncertainty is approximately 2.20 °C or 0.75% of the reading, whichever is greater.

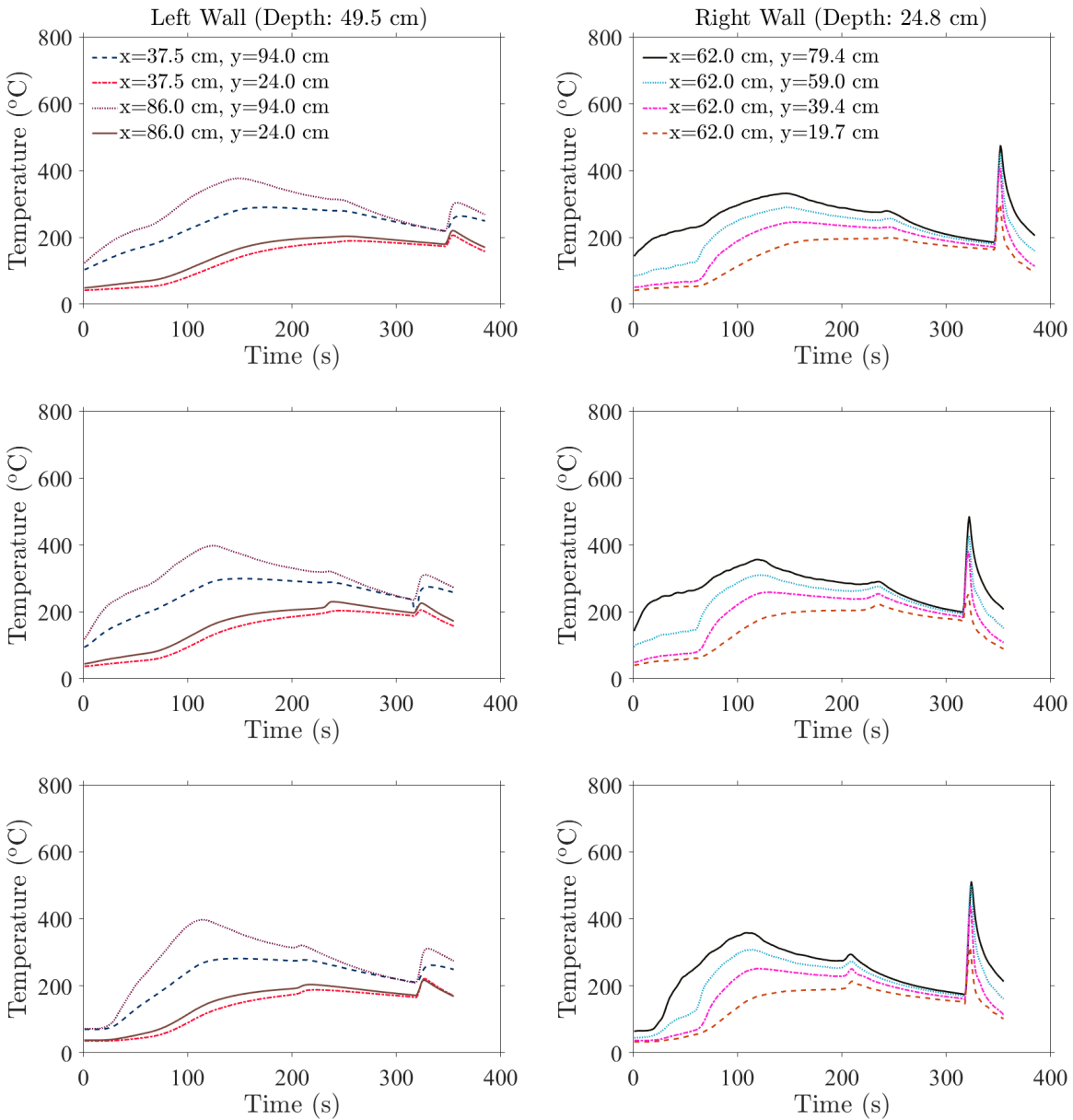


**Fig. 3.** Real-time temperature measurements of the 16.7 kW propane fire with a fuel flow time of 315 s (top), the 20.9 kW propane fire with a fuel flow time of 285 s (middle), and the 25.0 kW propane fire with a fuel flow time of 285 s (bottom) at different positions within the compartment. The expanded uncertainty of the temperature measurement estimated from the Type B evaluation of standard uncertainty is approximately 2.20 °C or 0.75% of the reading, whichever is greater.

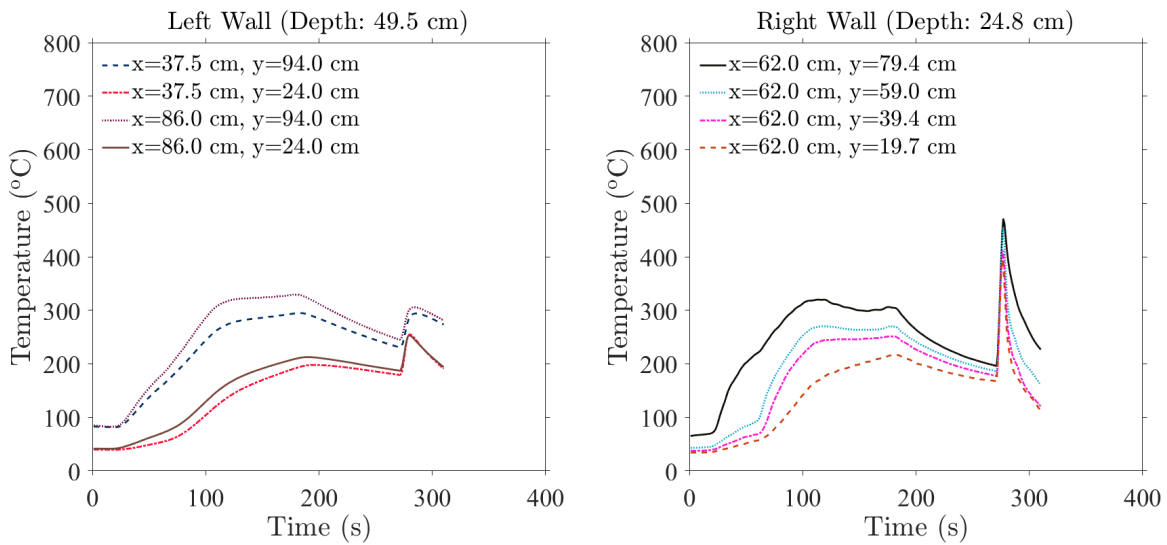


**Fig. 4.** Real-time temperature measurements of a 25.0 kW propylene fire with a fuel flow time of 270 s at different positions within the compartment. The expanded uncertainty of the temperature measurement estimated from the Type B evaluation of standard uncertainty is approximately 2.20 °C or 0.75% of the reading, whichever is greater.

### 3.1.2. Time-Averaged temperature measurements

Time-Averaged temperature measurements are presented in Figs. 5, 6, and 7 for experiments utilizing methane, propane, and propylene, at different fire sizes and fuel flow times, respectively. Time-average measurements were estimated from the mean averaged temperature measurements in repeated experiments subjected to the same conditions. Each experiment determined averaged temperature measurements from readings recorded 10 s before the doorway opening. The uncertainty of the time-averaged temperature measurements was estimated from a combined Type A and Type B evaluations of standard uncertainty, as detailed in Appendix B.

Compared to the real-time data shown in Figs. 2, 3, and 4, the time-averaged data for the methane, propane, and propylene fires follow a similar trend. The temperature decreases the longer the duration from when the initial flame is extinguished. Furthermore, as the fuel flow time increases, time-averaged temperatures at various positions converge to a constant value suggesting a bulk fluid temperature within the compartment.

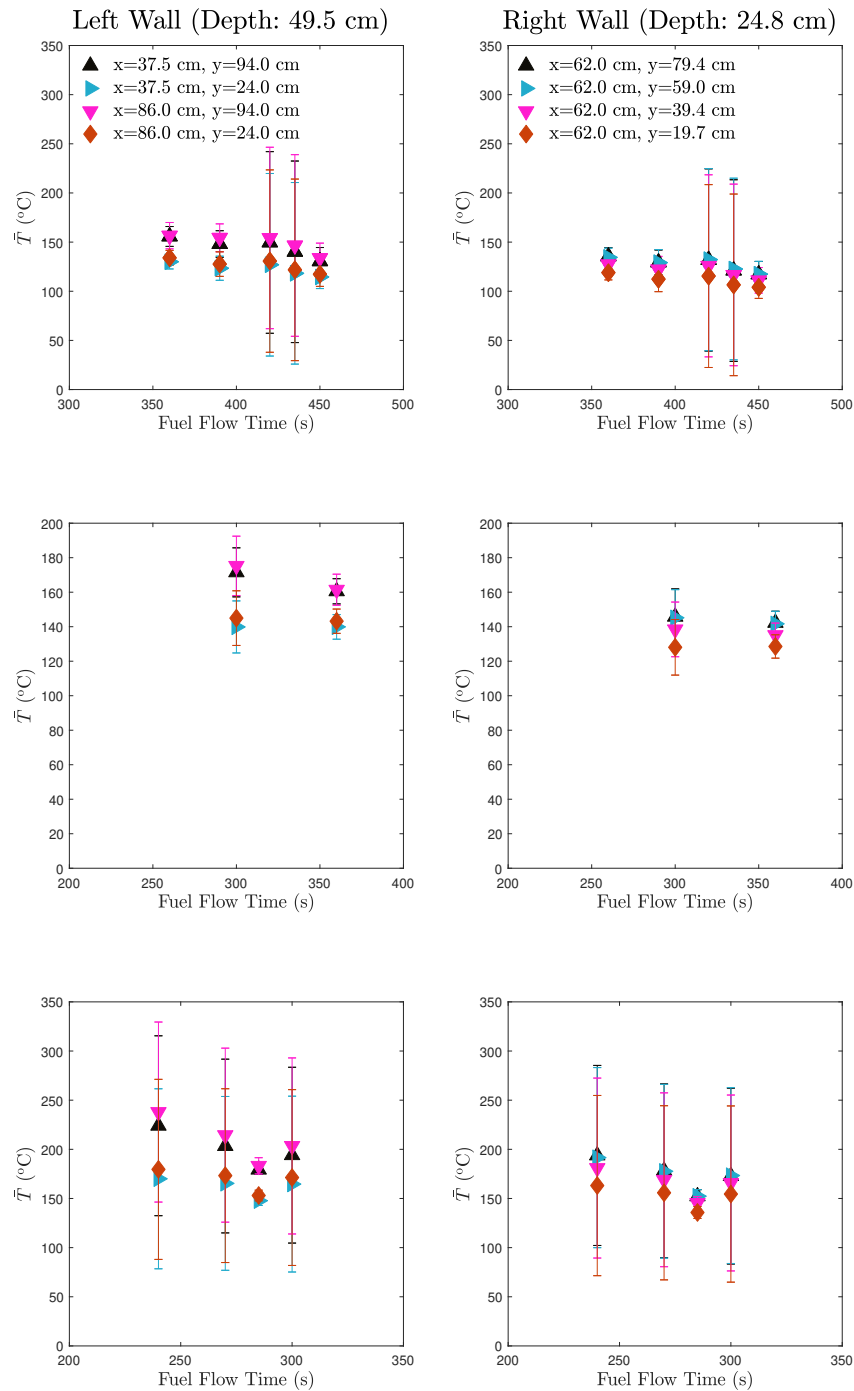


**Fig. 5.** Time-averaged temperature measurements of the 25.0 kW (top), 31.3 kW (middle), and 37.5 kW (bottom) methane fires with different fuel flow times at different positions within the compartment. The combined uncertainty of the time-averaged temperature measurement is estimated from a combination of the Type A and B evaluations of standard uncertainty.

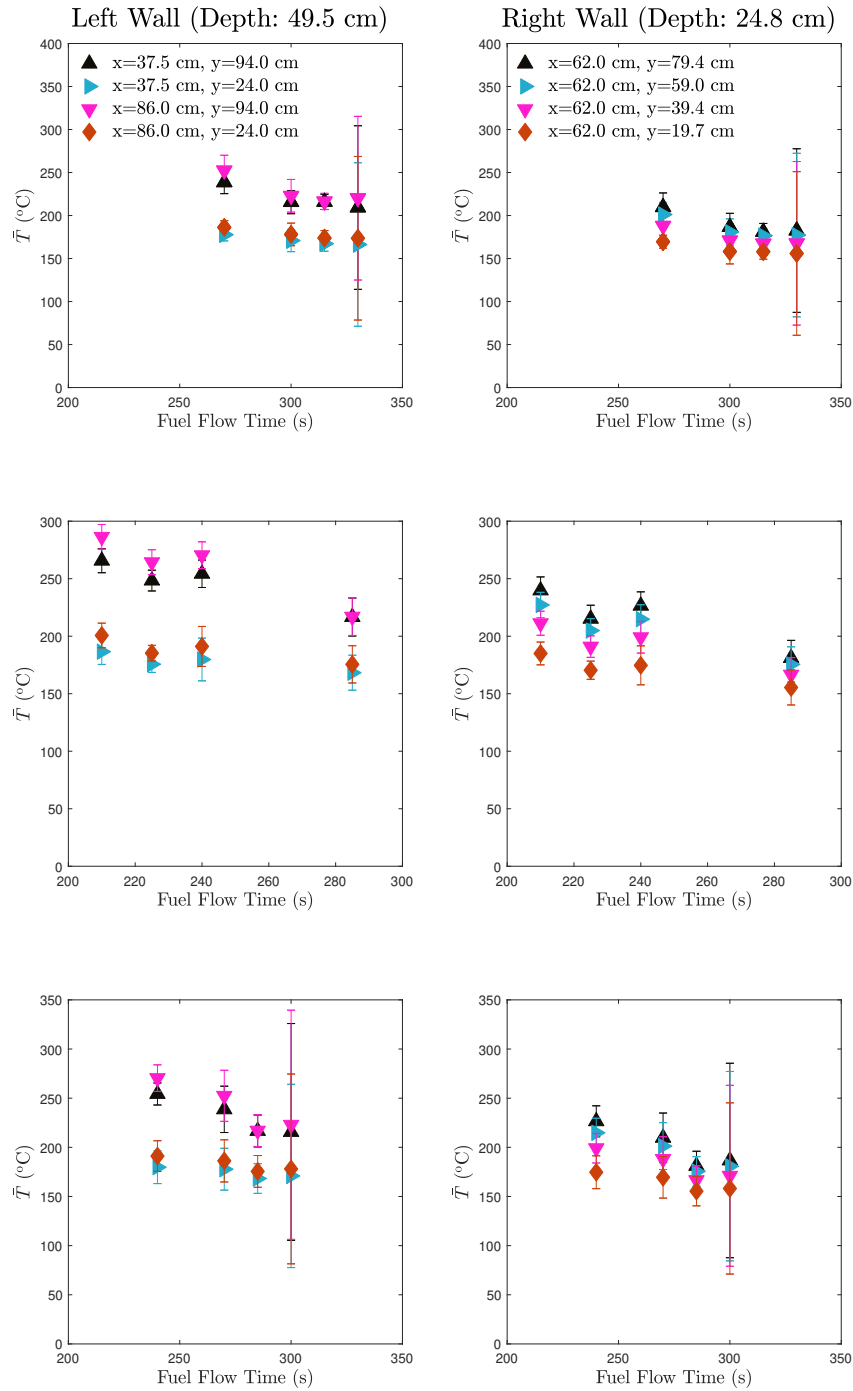


**Fig. 6.** Time-averaged temperature measurements of the 16.7 kW (top), 20.9 kW (middle), and 25.0 kW (bottom) propane fires with different fuel flow times at different positions within the compartment. The combined uncertainty of the time-averaged temperature measurement is estimated from a combination of the Type A and B evaluations of standard uncertainty.

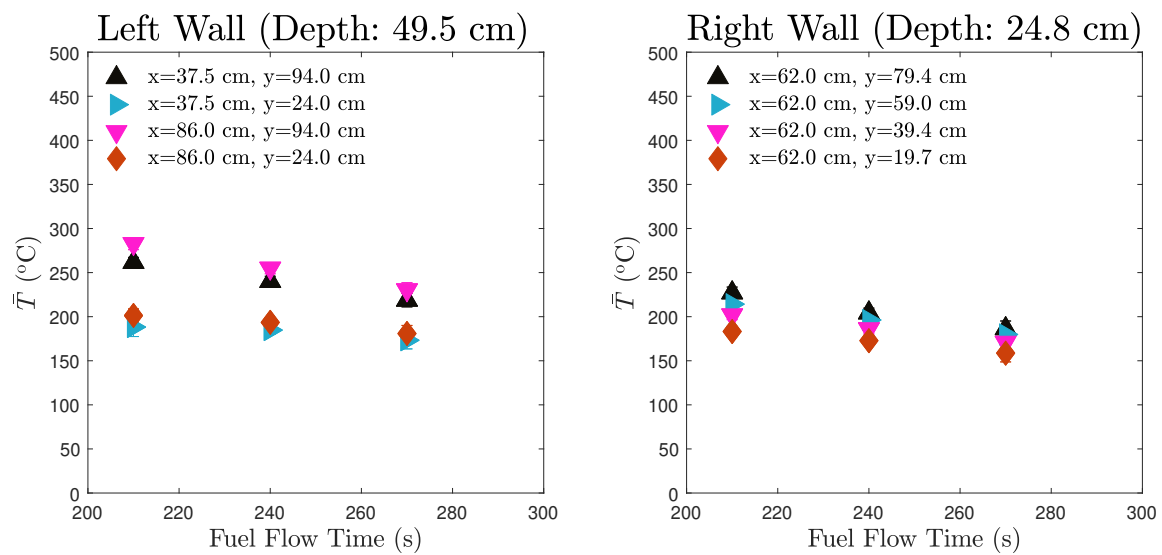


**Fig. 7.** Time-averaged temperature measurements of the 25.0 kW propylene fire with different fuel flow times at different positions within the compartment. The combined uncertainty of the time-averaged temperature measurement is estimated from a combination of the Type A and B evaluations of standard uncertainty.

## 3.2. Gas mixture composition measurements

### 3.2.1. Real-Time gas mixture composition measurements

Real-time gas mixture composition measurements are presented in Fig. 8 for a 25.0 kW, 31.3 kW, and 37.5 kW methane fire with various fuel flow times and at different positions within the compartment. Gas mixture composition measurements include the global and local equivalence ratios and gas concentrations of O<sub>2</sub>, CO<sub>2</sub>, and CO. Gas measurements were obtained at two positions for each experiment, indicating that Fig. 8 is a compilation of three experiments under the same condition but with different points of interest.

The gas mixture composition measurements follow a similar trend for different methane fire sizes. Initially, after ignition ( $t=0$  s), the global and local equivalence ratios are close to 0 at all positions as the doorway remains open. As the fire continues to burn in a quiescent environment, smoke is continuously building its presence in the upper compartment region, attributing to the rate of decline in O<sub>2</sub> and increase in CO<sub>2</sub> and CO concentrations. As the doorway shuts ( $t=60$  s), the oxygen declining rate increases with height. The global and local equivalence ratio also increases, signifying the growing concentration of unburned fuel, carbon dioxide, and carbon monoxide throughout the compartment.

As the compartment remains isolated, the local equivalence ratio increases faster than the global equivalence ratio, suggesting an accelerated presence of unburned fuel. As discussed in Ref [24], the global equivalence ratio is defined by the ratio of the total unburned and burned fuel to the total unburned and burned oxygen. The local equivalence ratio is determined by the ratio of only unburned fuel and oxygen. The discrepancy between the climb of the local and global equivalence ratio indicates an increasing presence of unburned fuel within the compartment that outpaces the fire's carbon dioxide and carbon monoxide generation.

For all fire configurations, at approximately  $200 \text{ s} \pm 20 \text{ s}$ , the flame extinguishes as observed via boroscope. The extinguished flame may attribute to the gas mixture near the burner falling below the limiting oxygen concentration for methane in the presence of combustion products, approximately  $14.5\% \pm 1\%$  [27]. Oxygen concentration values at the lowest sampling height drop below the limiting oxygen concentration at approximately the same time the flame extinguishes.

The absence of a flame, while methane continues to flow into the compartment, increases the global and local equivalence ratio's growth rate while staggering the generation of carbon dioxide and carbon monoxide. Oxygen concentrations are observed to briefly increase, caused by minor ventilation in the compartment's vent and creases. When the fuel stops flowing into the compartment 30 s before the doorway opens, the gas mixture composition measurements are nominally equivalent, except for the leaner mixtures observed close to the compartment floor ( $y < 30.0$  cm).

Upon the doorway opening, the equivalence ratios are observed to decline rapidly. Lower

compartment regions display a rapid drop in the equivalence ratios sooner than higher positions, suggesting that the gravity current penetrates the compartment closer to the floor, then mixes upward as it reaches the rear. A series of images depicting the flame propagation once the door opens of experiments subjected to 25 kW methane, propane, and propylene fires at different fuel flow times are shown in Fig. 9. For experiments involving methane, backdrafts were observed to propagate in the compartment's upper region, which further supports the sudden oxygen drop at the highest sampling position ( $y=90.0$  cm).

Notable differences are observed between gas mixture composition measurements for different methane fire sizes. The global and local equivalence ratio increase is found to be faster with fire size. Higher equivalence ratios and gas concentration peaks are observed in experiments with larger methane fire sizes.

As shown in Fig. 10, experiments that utilized propane at different fire sizes displayed a similar trend to methane fires before the fire extinguishing. Once the propane flame is extinguished, the local equivalence ratio increases faster in the compartment's middle layer ( $y=49.5$  cm) and closer to the front of the compartment ( $x=37.5$  cm). The higher local equivalence ratio in the middle layer of the compartment ( $y\sim 50.0$  cm), closer to the doorway, could attribute to the absence of oxygen and presence combustion products, as shown in the high carbon dioxide and carbon monoxide concentrations at the same position.

As the propane flow is shut off, a richer local equivalence ratio is measured closer to the compartment floor ( $y<30.0$  cm), indicating unburned fuel descending lower within the compartment. When the doorway opens, the local equivalence ratio is observed to spike at gas sampling positions lower in the compartment. The richer mixture residing in the bottom region of the compartment suggests that more fuel is present when the gravity current mixes into the enclosure resulting in flame propagating throughout the compartment as opposed to the upper region as observed in experiments involving methane. The larger span of the propane flame is demonstrated in Fig. 9 which shows the flame growth throughout the compartment, including lower regions relative to the methane fire experiments.

At the compartment's lowest sampling position ( $y=22.0$  cm), the global and local equivalence ratio peaks increase with propane fire size. The local equivalence ratio at the middle sampling position ( $y=49.5$  cm), closer to the doorway ( $x=37.5$  cm), is shown to peak with increasing fire size at the approximate time the initial flame is extinguished. Carbon monoxide concentrations are also found to peak close to the compartment floor ( $y<35.0$  cm) during a backdraft, further supporting the fuel-rich mixture in the lower layer of the compartment when the doorway opens.

Gas mixture composition measurements obtained in experiments utilizing a 25 kW propylene fire were only taken at two sampling locations. The limited dataset is presented in Fig. 11. Measurement profiles of the 25 kW propylene fire were observed to follow similar trends to that of experiments involving the 25 kW propane fire. Equivalence ratios were higher at the lower sampling position, indicating a richer mixture close to the compartment floor when the doorway opens. The local equivalence ratio and carbon monoxide

concentrations peak during a backdraft, suggesting a richer fuel mixture as the gravity current flows into the enclosure. As the doorway opens, the rich lower region is further made evident through visual observation of flame geometry, which propagated throughout the compartment during a backdraft, as shown in Fig. 9.

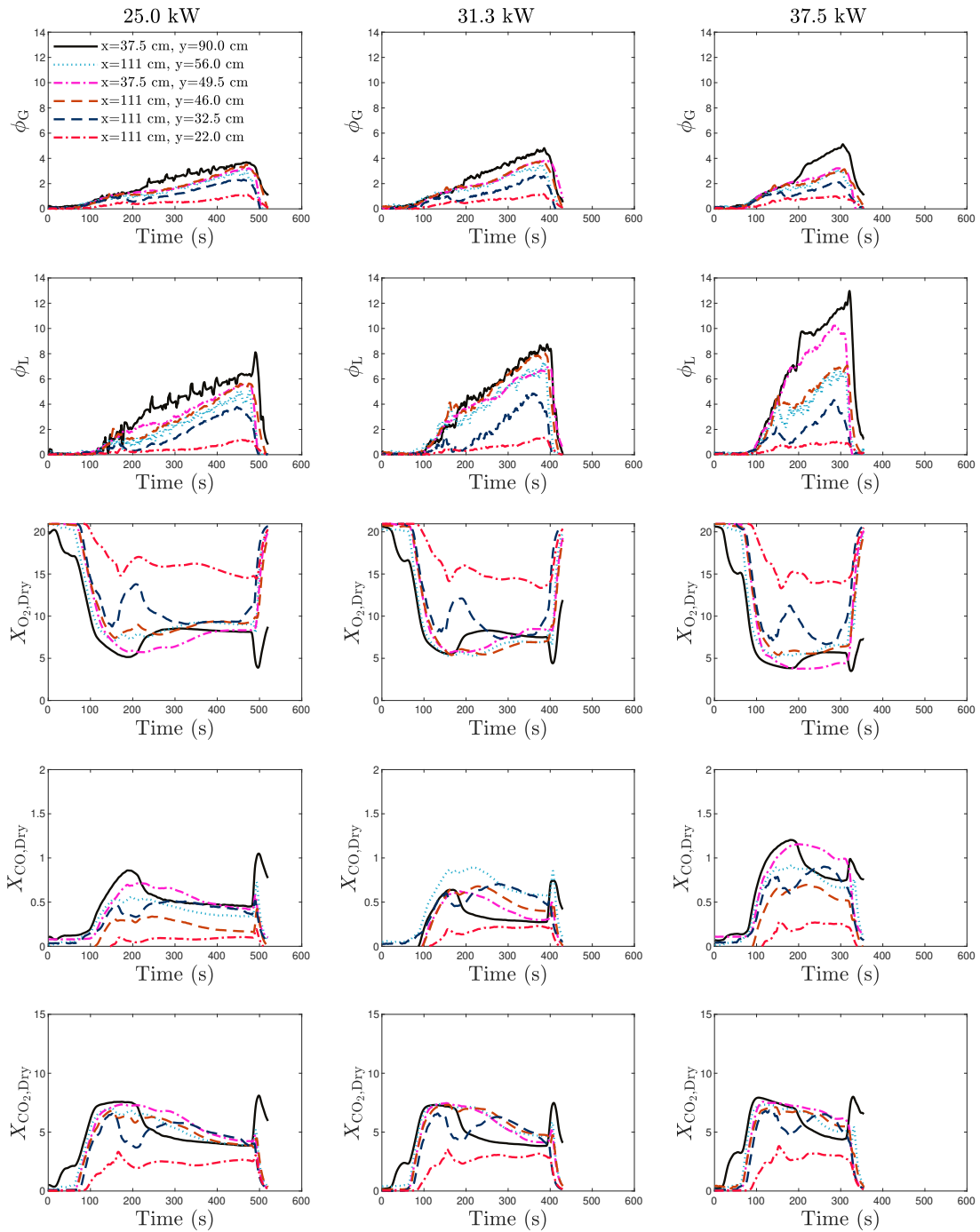


**Fig. 8.** Real-time gas mixture composition measurements of the 25.0 kW methane fire with a fuel flow time of 450 s (left), the 31.3 kW methane fire with a fuel flow time of 360 s (center), and the 37.5 kW methane fire with a fuel flow time of 285 s (right) at different positions within the compartment. The uncertainty of the gas mixture composition measurements is described in Appendix A.

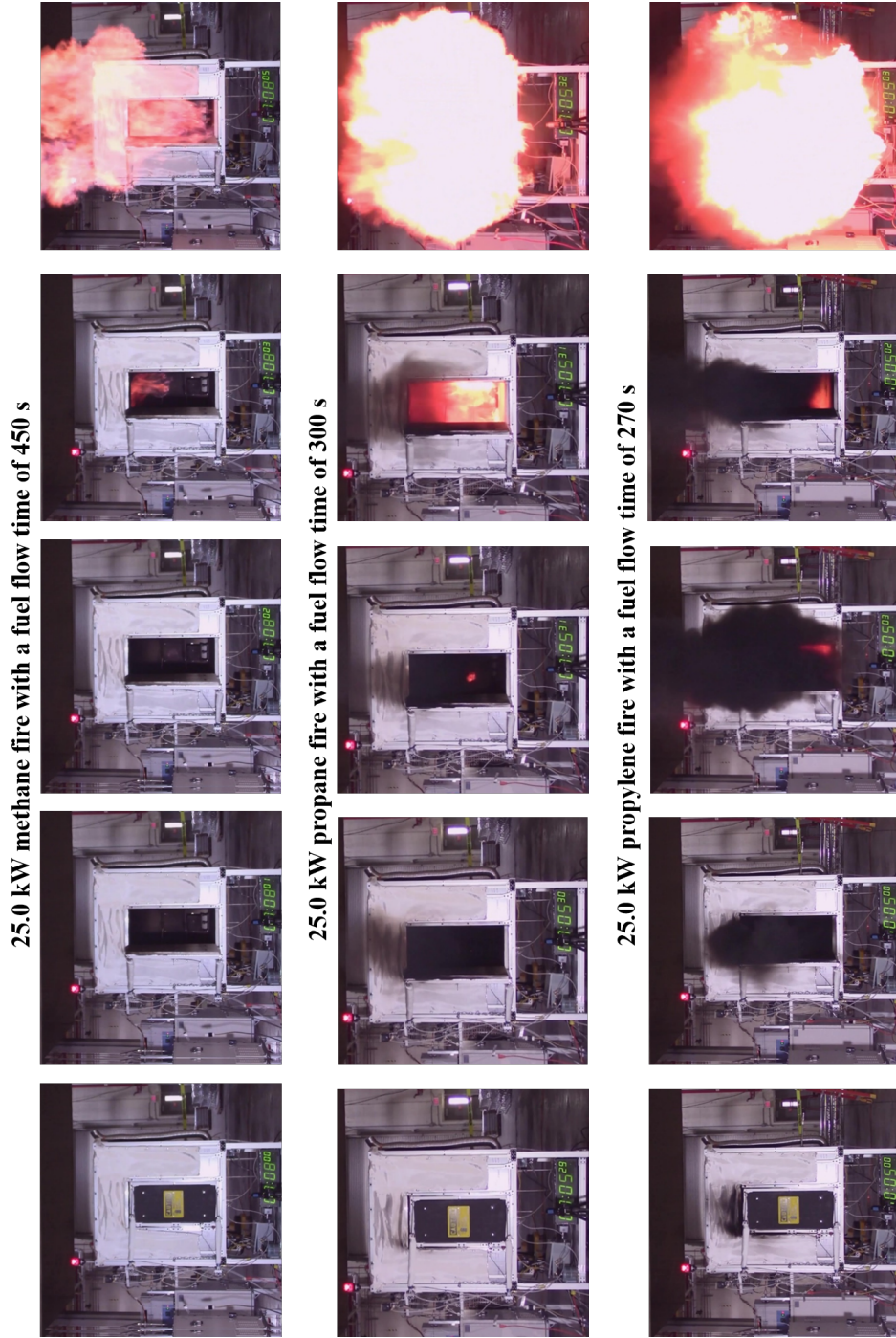


**Fig. 9.** Sequences of flame propagation in the compartment previously subjected to 25.0 kW methane, propane, and propylene fires with a fuel flow time of 450 s, 300 s, and 270 s, respectively. For each presented experiment, the compartment is configured with a low spark igniter position.

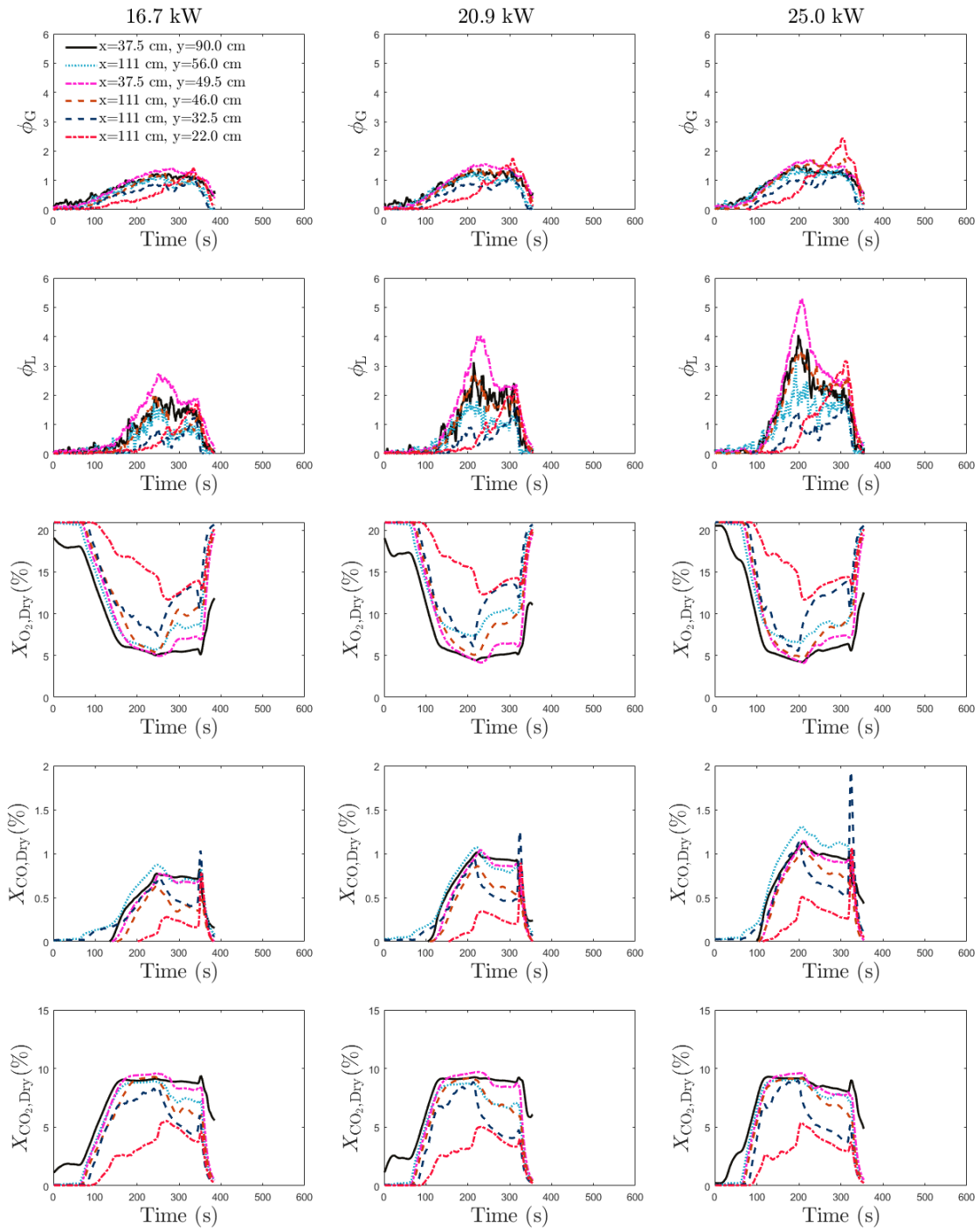


**Fig. 10.** Real-time gas mixture composition measurements of the 16.7 kW propane fire with a fuel flow time of 315 s (left), the 20.9 kW propane fire with a fuel flow time of 285 s (center), and the 25.0 kW propane fire with a fuel flow time of 285 s (right) at different positions within the compartment. The uncertainty of the gas mixture composition measurements is described in Appendix A.

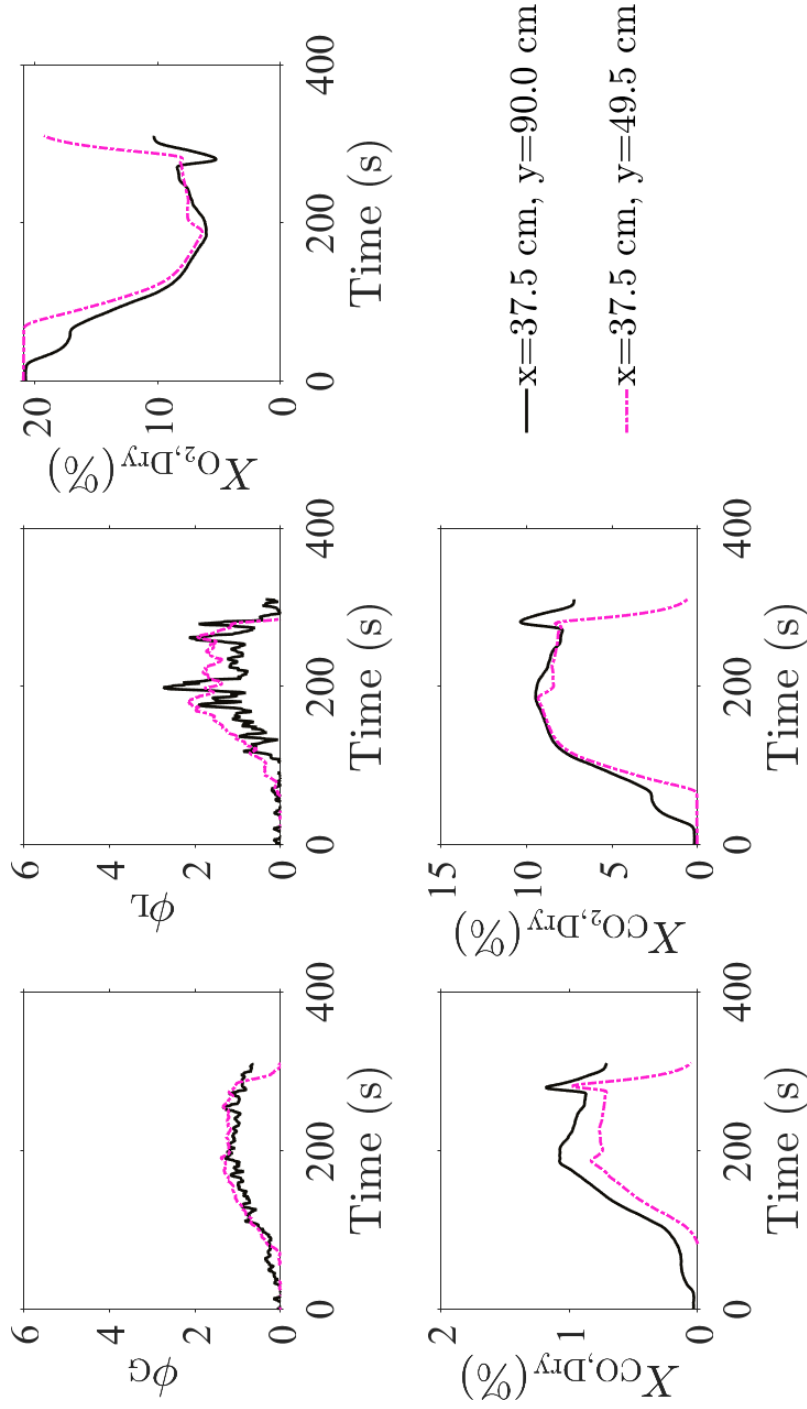


**Fig. 11.** Real-time gas mixture composition measurements of a 25.0 kW propylene fire with a fuel flow time of 270 s at different positions within the compartment. The uncertainty of the gas mixture composition measurements is described in Appendix A.

### 3.2.2. Time-Averaged gas mixture composition measurements

Figures 12, 13, and 14 display the time-averaged gas mixture composition measurements for experiments utilizing methane, propane, and propylene fires of different sizes and fuel flow times, respectively. Time-average measurements were estimated from the mean averaged gas mixture composition measurements made in repeated experiments subjected to the same conditions. Each experiment determined averaged gas mixture composition measurements from readings recorded 10 s prior to the doorway opening. The uncertainty of the time-average gas mixture composition measurements was estimated from a combined Type A and B evaluations of standard uncertainty. Further details are described in Appendix B.

When presented as a function of fuel flow time, the time-averaged gas mixture composition measurements mimic trends displayed in Figs. 8, 10, 11. The global and local equivalence ratios increase with fuel flow time in instances where the parent fuel is methane. The local equivalence ratio is nominally consistent in the middle region of the compartment ( $y \sim 50.0$  cm) for most configurations. Time-averaged oxygen concentrations at the lowest sampling position are approximately  $15\% \pm 0.5\%$  for all fire sizes and fuel flow times. Time-averaged carbon monoxide and carbon dioxide concentration measurements are nominally consistent in the upper region of the compartment ( $y > 50$  cm) regardless of fuel flow time and are observed to increase with fire size.

Time-averaged gas mixture composition measurements for experiments involving propane fires at various fuel flow times are shown in Fig. 13. Compared to methane experiments, the time-averaged global and local equivalence ratio measurements obtained in experiments with propane fires are lower and are observed to converge to an approximate value as the fuel flow time increases. Oxygen concentrations are observed to be higher closer to the compartment floor. Carbon dioxide and carbon monoxide measurements are shown to reiterate observations from Fig. 10 in that the concentrations remain relatively constant in the upper region of the compartment ( $y > 50.0$  cm) but a decline in the lower region as the fuel flow time increase.

Figure 14 presents the time-averaged gas mixture composition measurements at two sampling locations for experiments utilizing a 25 kW propylene fire. The relationship between the gas mixture composition measurement and fuel flow time is similar to propane experiments. The difference between equivalence ratio measurements decreases with an increase in fuel flow time. Carbon dioxide and carbon monoxide concentration measurements are independent of fuel flow time.

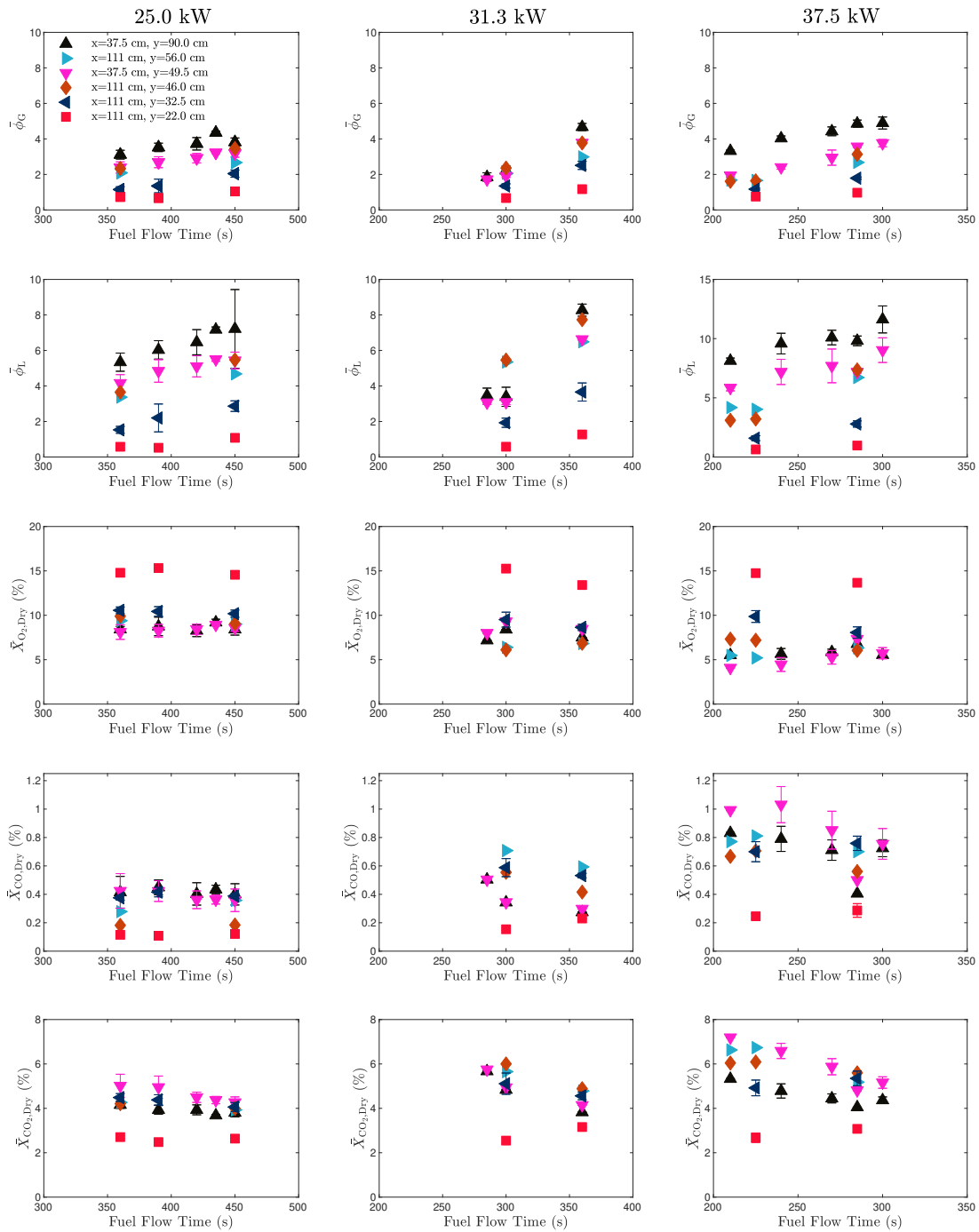


**Fig. 12.** Time-averaged gas mixture composition measurements of the 25.0 kW, 31.3 kW, and 37.5 kW methane fires with different fuel flow times at different positions within the compartment. The time-averaged gas mixture composition's combined uncertainty is estimated from a combination of the Type A and B evaluations of standard uncertainty. Uncertainty analysis of the time-averaged gas mixture concentration measurements is provided in Appendix B.

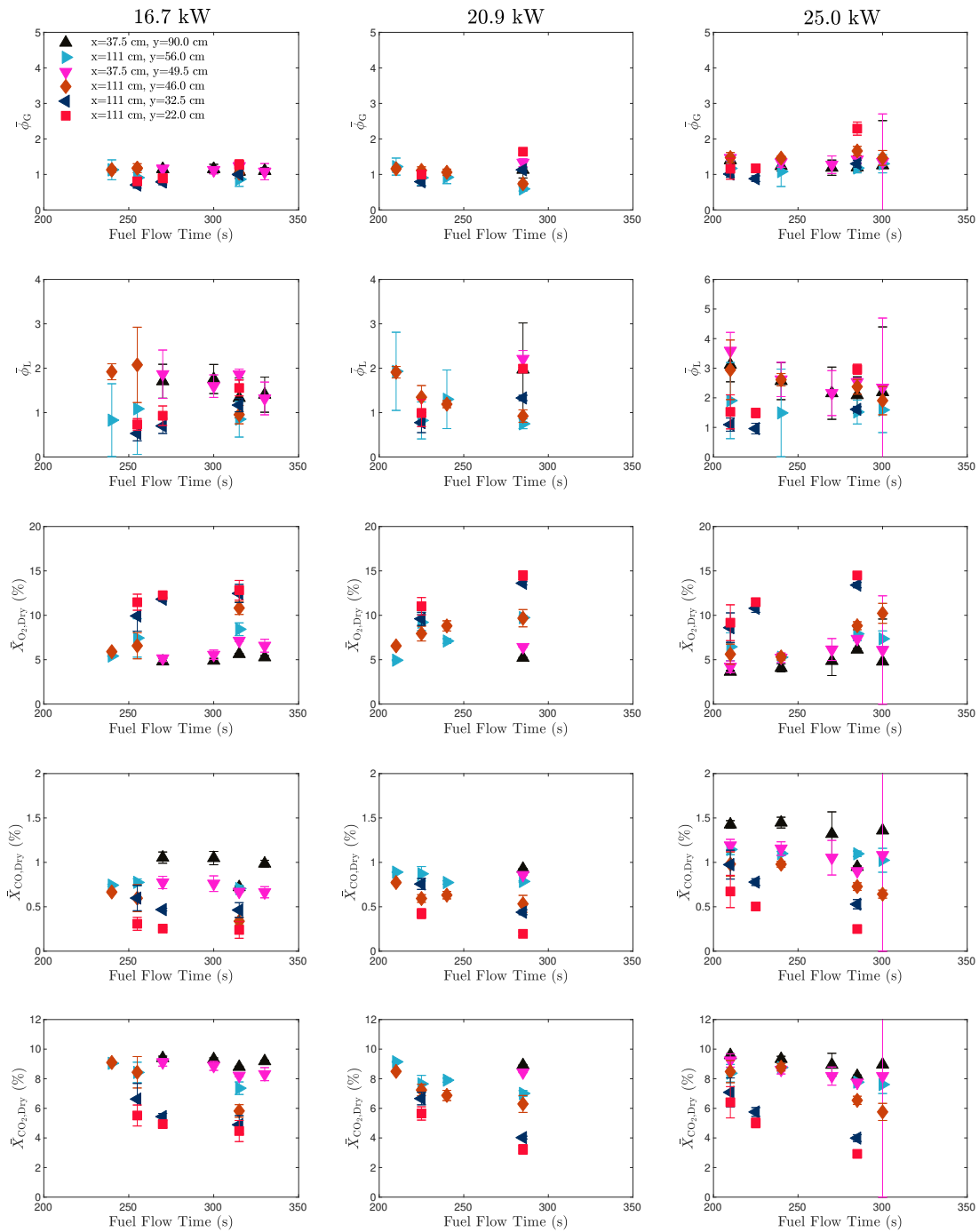


**Fig. 13.** Time-averaged gas mixture composition measurements of the 16.7 kW, 20.9 kW, and 25.0 kW propane fires with different fuel flow times at different positions within the compartment. The combined uncertainty of the time-averaged gas mixture composition measurements is estimated from a combination of the Type A and B evaluations of standard uncertainty. Uncertainty analysis of the time-averaged gas mixture concentration measurements is provided in Appendix B.

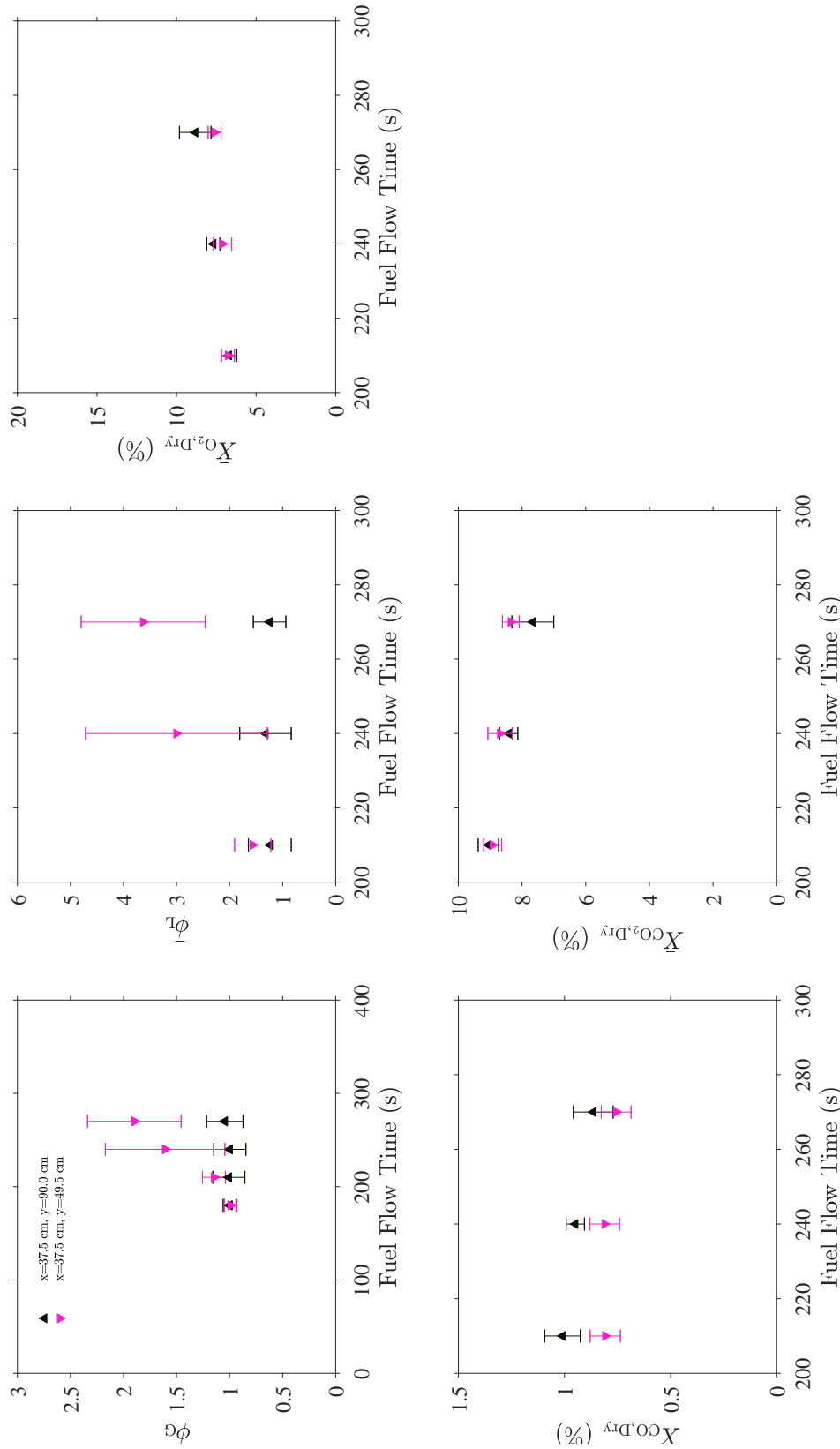


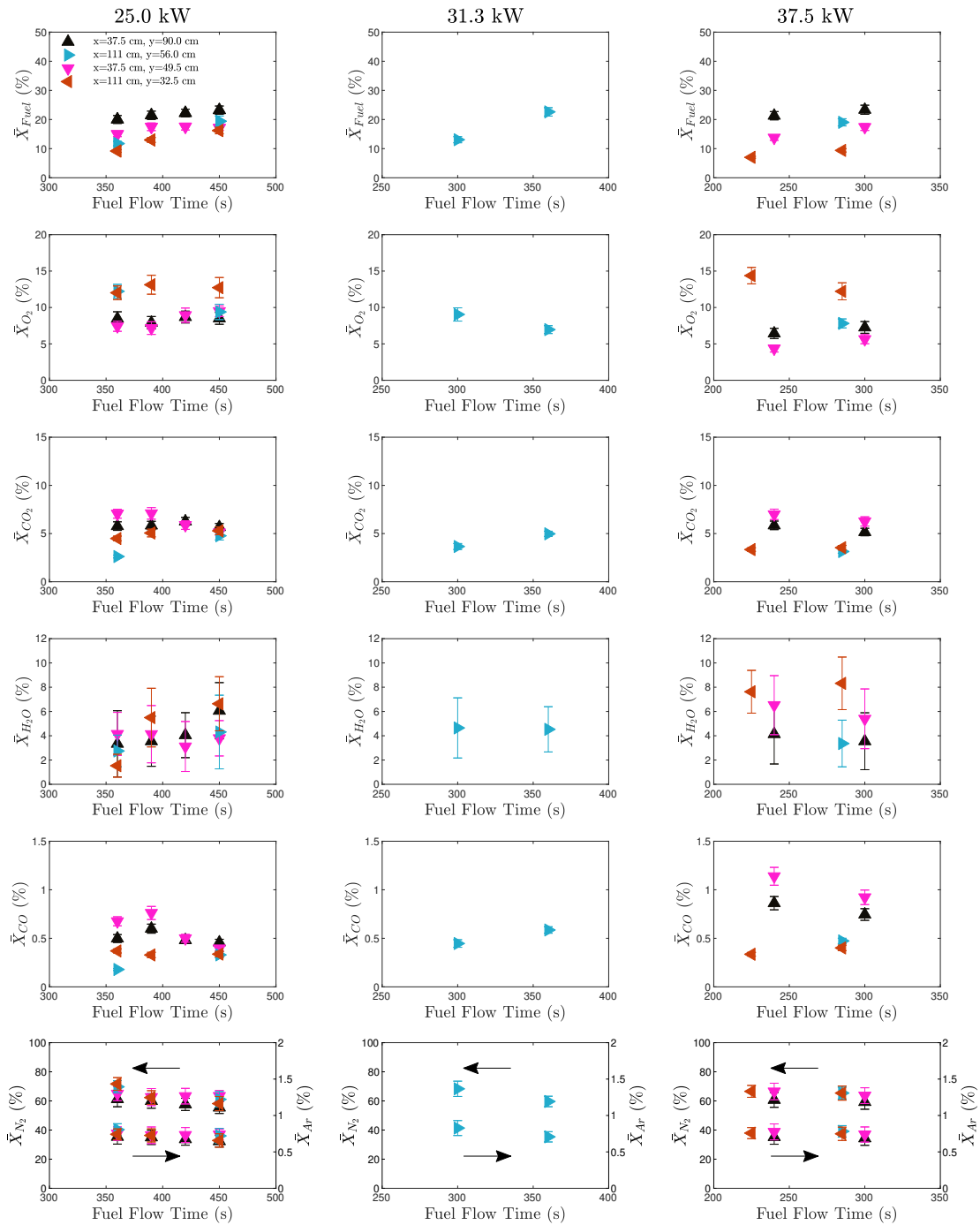
**Fig. 14.** Time-averaged gas mixture composition measurements of the 25.0 kW propylene fire with different fuel flow times at different positions within the compartment. The combined uncertainty of the time-averaged gas mixture composition measurements is estimated from a combination of the Type A and B evaluations of standard uncertainty. Uncertainty analysis of the time-averaged gas mixture concentration measurements is provided in Appendix B.

A more detailed description of the gas mixture composition is provided in the time-averaged gas species concentration measurements determined via GC/MSD. The time-averaged species concentration measurements are presented in Fig 15, 16, and 17 for experiments utilizing methane, propane, and propylene, respectively, at different fire sizes and fuel flow times. In these figures, the concentration of fuel,  $\bar{X}_{\text{Fuel}}$ , is the sum of all unburned fuel species detected in the gas sample. In addition to the parent fuel, other unburned fuel species include trace amounts of acetylene, ethylene, ethane, and benzene. Low levels of propylene were observed in gas samples obtained from experiments involving propane and propylene as the parent fuels.

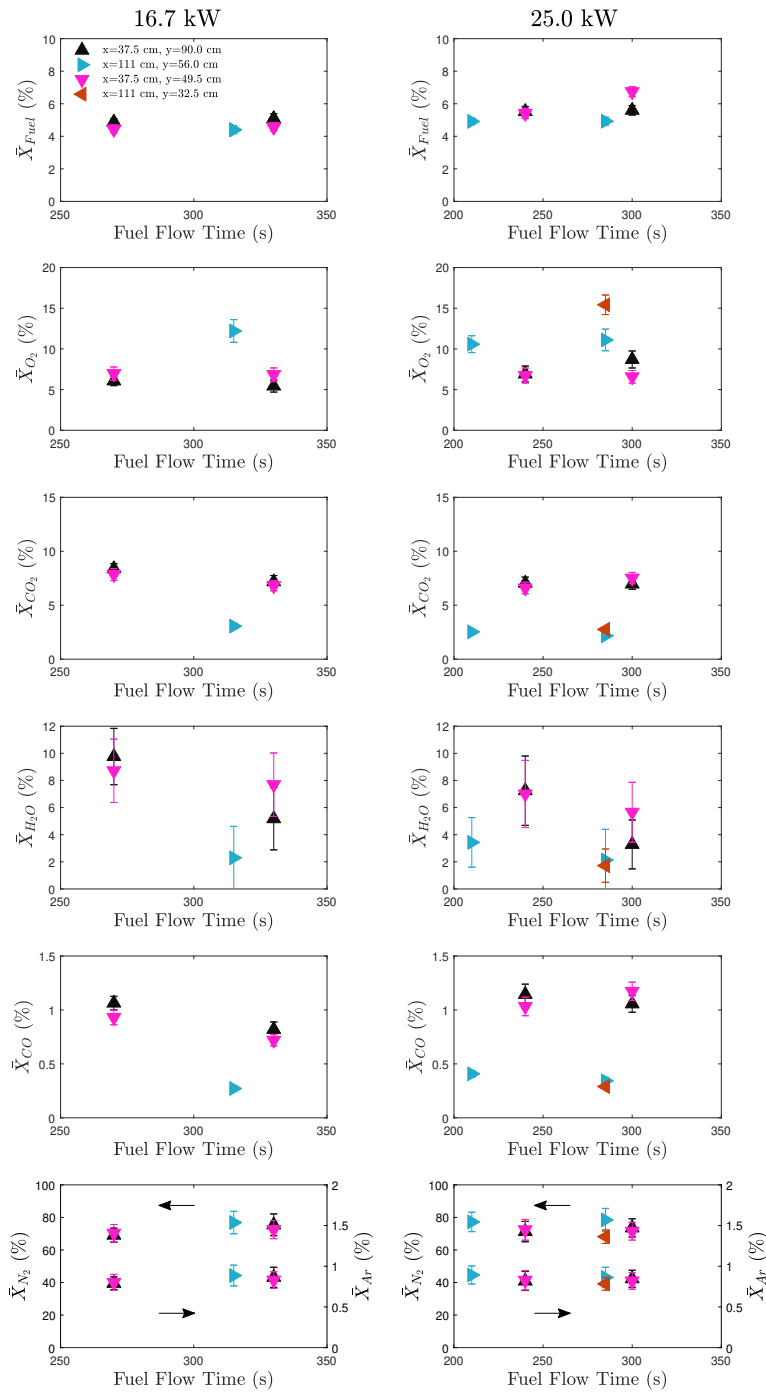
The time-averaged gas species measurements complement phi meter and gas analyzers' measurements for experiments implementing methane as the fuel source. The total fuel concentration is shown to increase at all positions as the fuel flow time increases, similar to how the global and local equivalence ratios increase in Fig 8. The fuel concentration is higher in the upper region of the compartment, closer to the doorway. Combustion products (i.e., carbon dioxide, water vapor, and carbon monoxide) and inerts (i.e., nitrogen and argon) are relatively steady as fuel flow time increases. Higher concentrations of water vapor are observed in instances with high oxygen concentrations. The highest carbon monoxide concentration is observed in the compartment's middle layer for every fuel flow time, as demonstrated by gas analyzer measurements in Figs. 8 and 12.

Figure 16 presents the time-averaged gas species measurements in experiments with the 16.7 kW and 25.0 kW propane fires at different fuel flow times. No gas samples were collected for the 20.9 kW propane fire. In both instances of different fire sizes, the fuel concentration is nominally constant regardless of the fuel flow time. Higher oxygen concentrations were measured in the lower region of the compartment ( $y < 50.0$  cm), farther back from the doorway ( $x = 111.0$  cm). Combustion product concentrations were higher at positions where the oxygen concentrations were low. The consistent concentrations of gas species at the same position but varying fuel flow time support previously described gas mixture composition measurements.

Extracted gas samples to be processed by the GC/MSD were acquired at only two positions for experiments with a 25 kW propylene fire. The time-averaged gas species concentrations are presented in Fig. 17. Gas species concentrations are consistent at the different fuel flow times.



**Fig. 15.** Time-averaged gas species concentration measurements obtained via GC/MSD of the 25.0 kW, 31.3 kW, and 37.5 kW methane fires with different fuel flow times at different positions within the compartment. The combined uncertainty of the time-averaged gas species concentration measurements is estimated from a combination of the Type A and B evaluations of standard uncertainty. Uncertainty analysis of the time-averaged gas species concentration measurements is provided in Ref [21].



**Fig. 16.** Time-averaged gas species concentration measurements obtained via GC/MSD of the 16.7 kW, 20.9 kW, and 25.0 kW propane fires with different fuel flow times at different positions within the compartment. The combined uncertainty of the time-averaged gas mixture composition measurements is estimated from a combination of the Type A and B evaluations of standard uncertainty. Uncertainty analysis of the time-averaged gas species concentration measurements is provided in Ref [21].

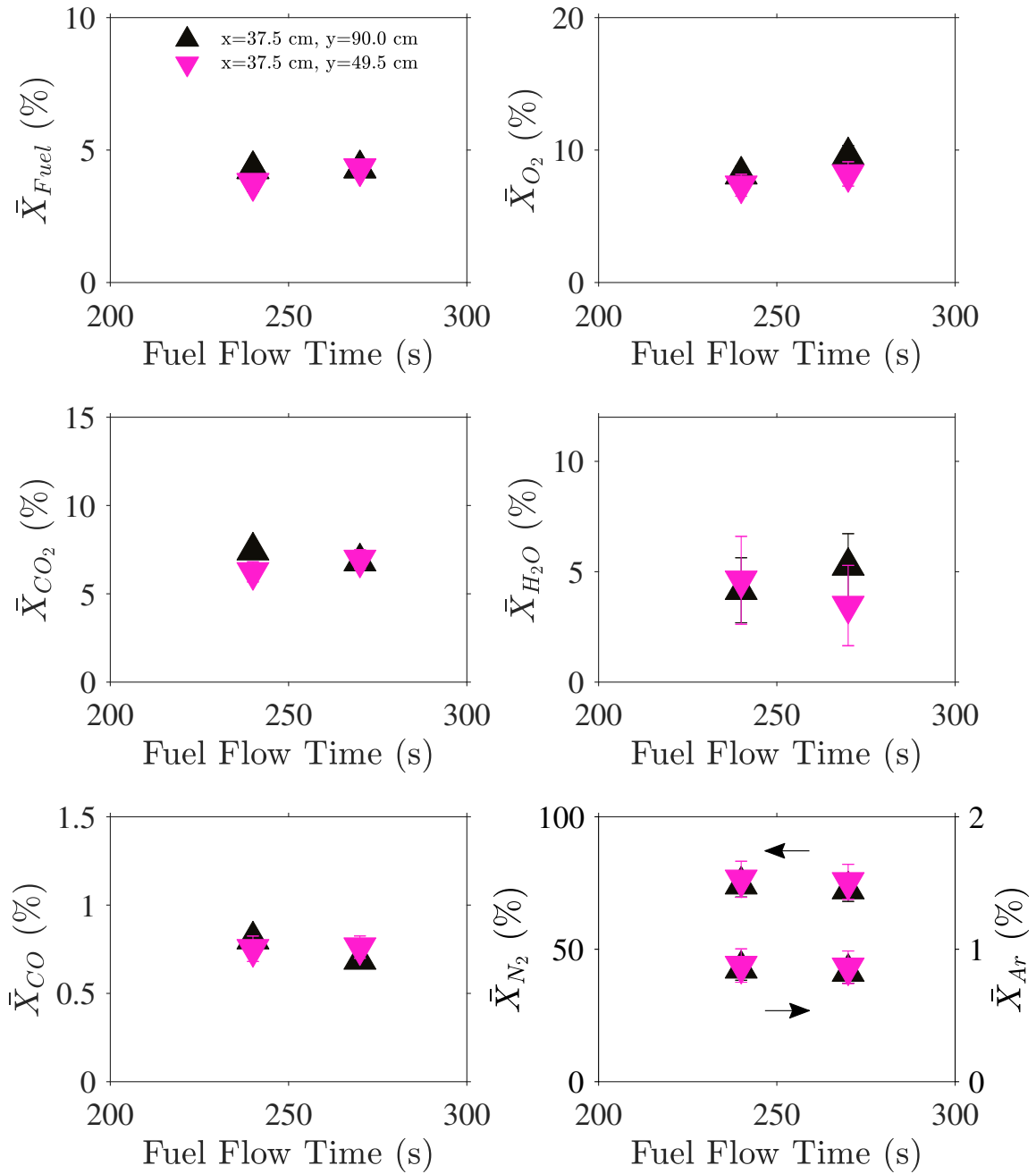


**Fig. 17.** Time-averaged gas species concentration measurements obtained via GC/MSD of the 25.0 kW propylene fires with different fuel flow times at different positions within the compartment. The combined uncertainty of the time-averaged gas mixture composition measurements is estimated from a combination of the Type A and B evaluations of standard uncertainty. Uncertainty analysis of the time-averaged gas species concentration measurements is provided in Ref [21].

#### 4. Verifying Gas Composition Measurements

Time-averaged measurements of the global and local equivalence ratios and gas concentrations of oxygen, carbon dioxide, and carbon monoxide were compared to measurements made via GC/MSD of an extracted gas sample. As discussed in Section 3.2.2, relatively small concentrations of stable hydrocarbons (i.e., ethane, ethylene, acetylene, benzene) were measured for fire configurations and were used to calculate the global and local equivalence ratio using Eqs. 3 and 4, respectively. The global equivalence ratio is calculated from GC/MSD measurements via the product of a stoichiometric coefficient and the ratio of the sum of all uncombusted fuels and combustion products to uncombusted oxygen and all combustion products derived from oxygen. The local equivalence ratio is calculated via the ratio between the sum of all unburned fuels and oxygen present in the extracted sample over the stoichiometric ratio of each fuel, assuming one mole of fuel, as shown in Eq. 4.

$$\bar{\phi}_G = \frac{(x + \frac{y}{4} - \frac{z}{2})}{x} \left( \frac{\sum(x + \frac{y}{4} - \frac{z}{2}) \cdot X_{i,C}}{X_{O_2} + X_{CO_2} + 0.5X_{CO} + 0.5X_{H_2O}} \right) \quad (3)$$

$$\bar{\phi}_L = \frac{\sum(x + \frac{y}{4} - \frac{z}{2}) \cdot X_{(C_xH_yO_z)}}{X_{O_2}} \quad (4)$$

Here,  $X_i$  represents the mole fraction of species  $i$ . The mole fraction of fuel is represented by  $X_{(C_xH_yO_z)}$  and  $x$ ,  $y$ , and  $z$  are the number of carbon, hydrogen, and oxygen atoms in the parent fuel. The concentration of carbon containing species derived from the parent fuel is represented by  $X_{i,C}$ . Gas concentration measurements obtained using the gas analyzer were compared to GC/MSD concentration measurements recalculated on a dry basis.

The comparison between the independent equivalence ratio and gas species concentration measurements is displayed in Fig. 18, with unity being represented by the dotted line. For most experiments, the time-averaged equivalence ratio estimated from the phi meter and GC/MSD is in fair agreement within experimental uncertainty. The oxygen, carbon dioxide, and carbon monoxide concentration measurements obtained from the gas analyzer and GC/MSD are also in fair agreement with some experimental uncertainty. The agreement between measurements validates the experimental technique and indicates minimal loss of condensable or semi-volatile species within the heated gas line.

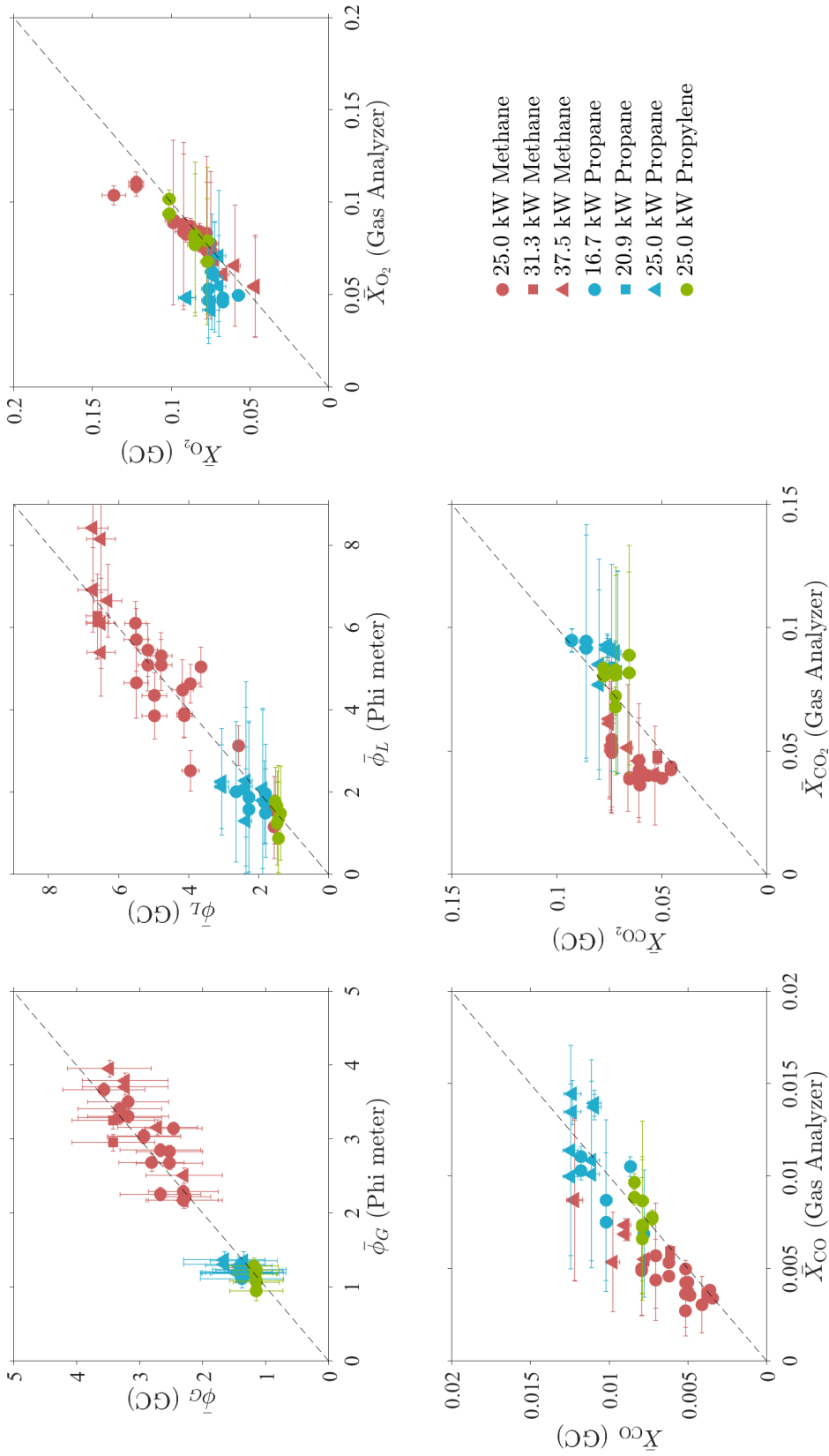


**Fig. 18.** Time-averaged gas mixture composition measurements were obtained via phi meter and gas analyzer compared to GC/MSD measurements. The provided uncertainties represent a combined Type A and B evaluations of standard uncertainty.

## 5. Probabilities of Backdraft at varying experimental conditions

The probability of a backdraft under a set compartment configuration (i.e., fuel type, fire size, spark location, doorway opening size) is presented in a series of conditional density plots, Figs. 19-25. Each plot represents the likelihood of backdraft as a function of fuel flow time at a fixed compartment configuration (i.e., fuel, fire size, "door" or "window" opening configuration, and lower or middle spark location). For all configurations, the probability of backdraft increases with the fuel flow time. Under the same fuel type and fuel flow time, the probability of a backdraft is greater when the spark location is higher in the compartment. Backdraft probabilities are also improved with a "window" opening configuration, 20% smaller than the whole doorway opening. The higher probability of backdraft under the smaller doorway and middle spark location conditions could be attributed to the turbulent mixing of the incoming gravity current, presenting a flammable mixture surrounding the spark igniter.

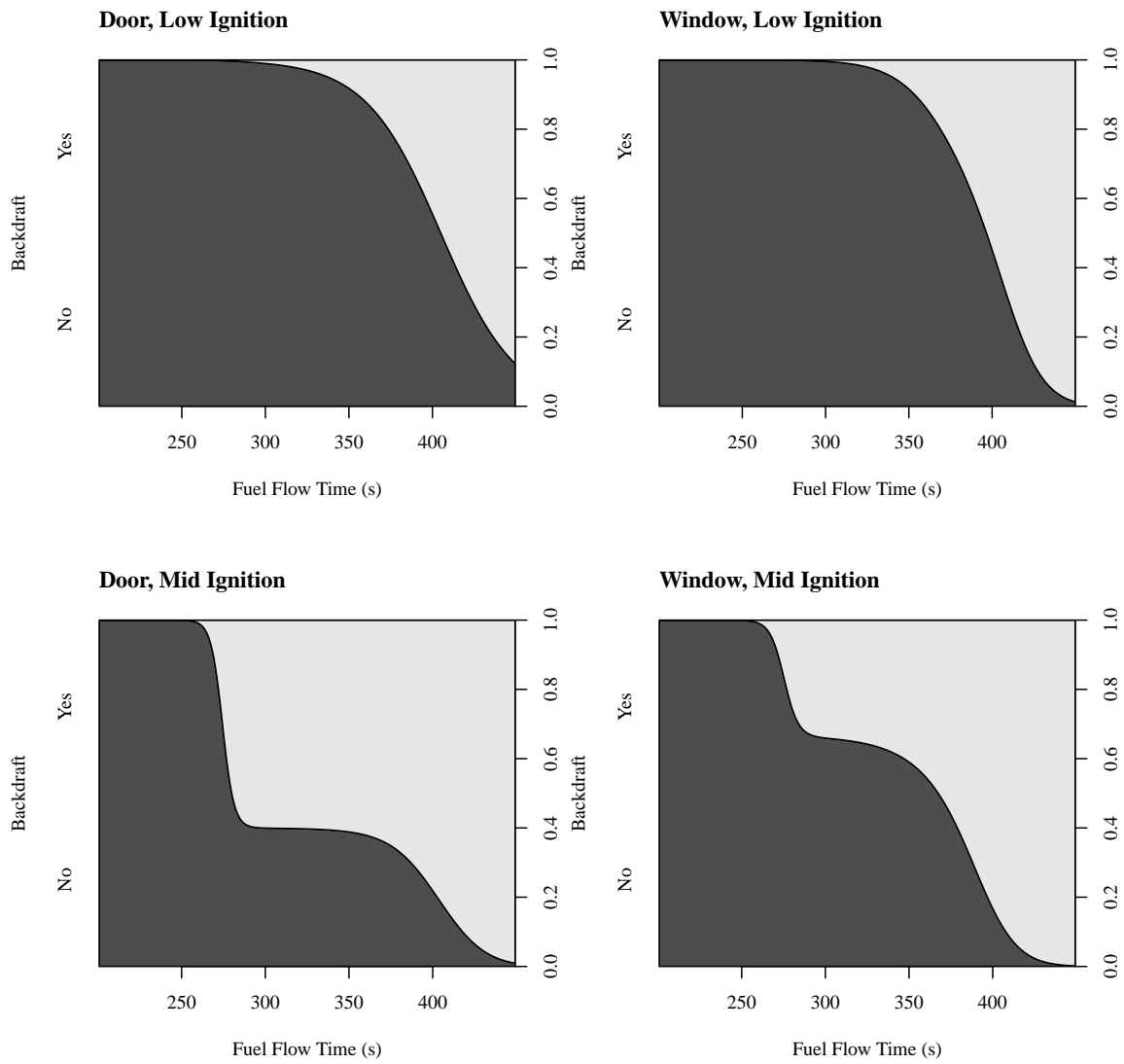


**Fig. 19.** Conditional density plot of a 25 kW methane fire as a function of fuel flow time at various compartment configurations

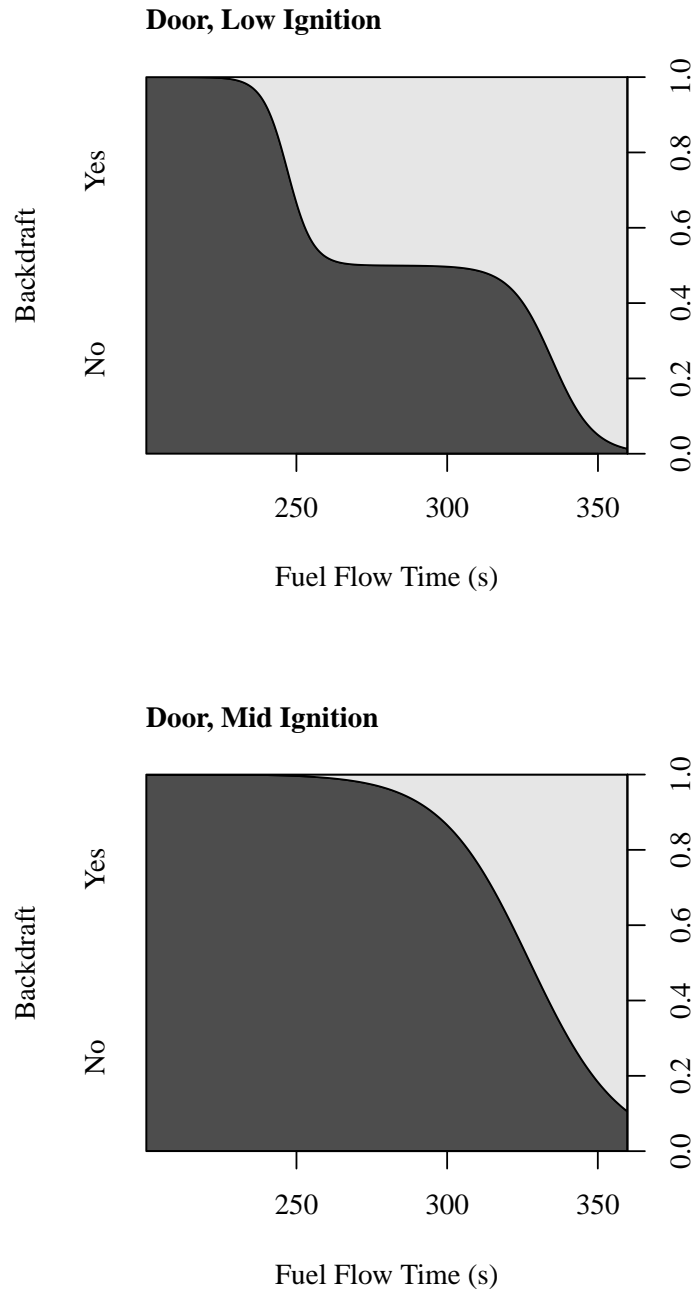


**Fig. 20.** Conditional density plot of a 31.3 kW methane fire as a function of fuel flow time at various compartment configurations

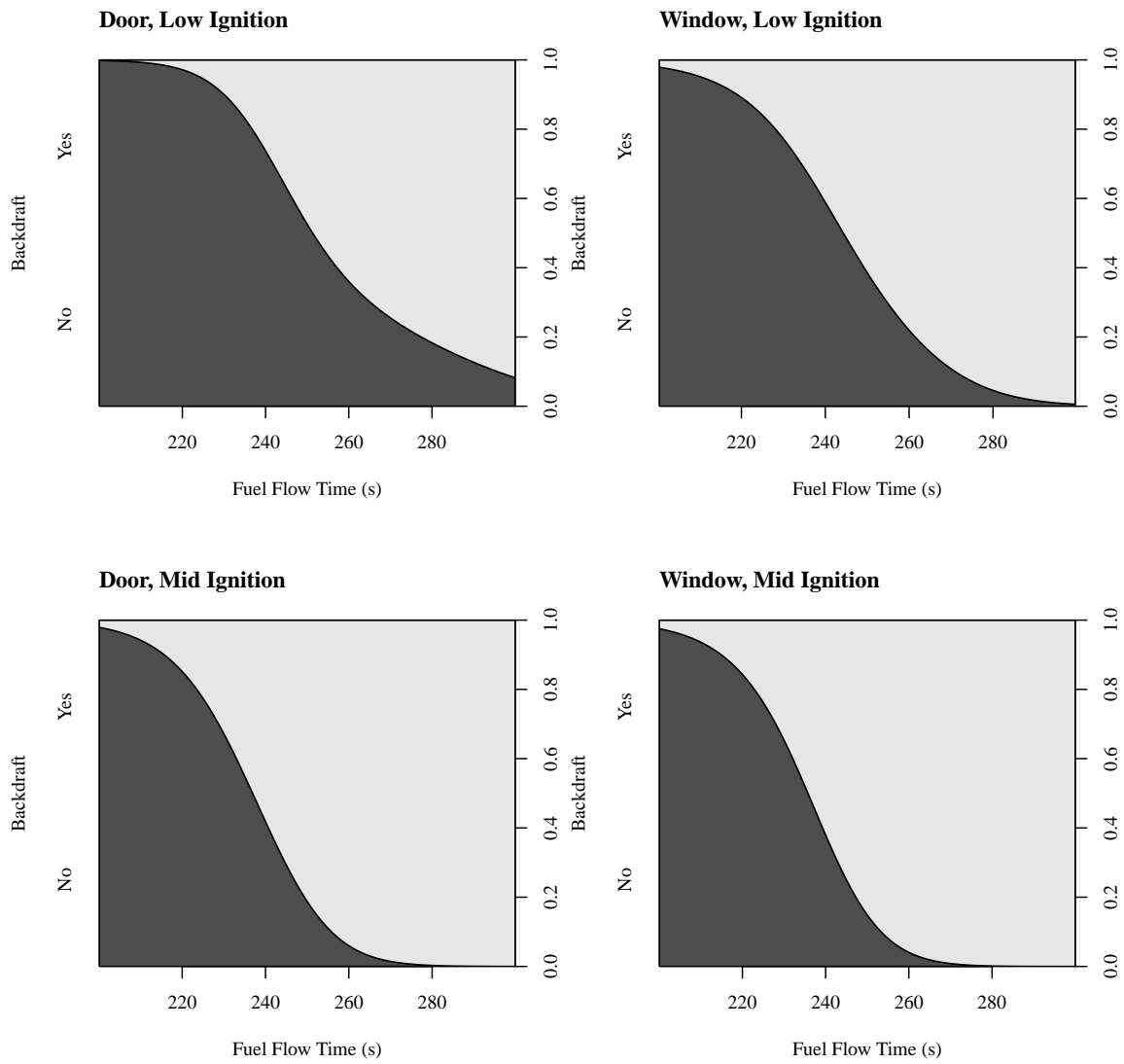


**Fig. 21.** Conditional density plot of a 37.5 kW methane fire as a function of fuel flow time at various compartment configurations

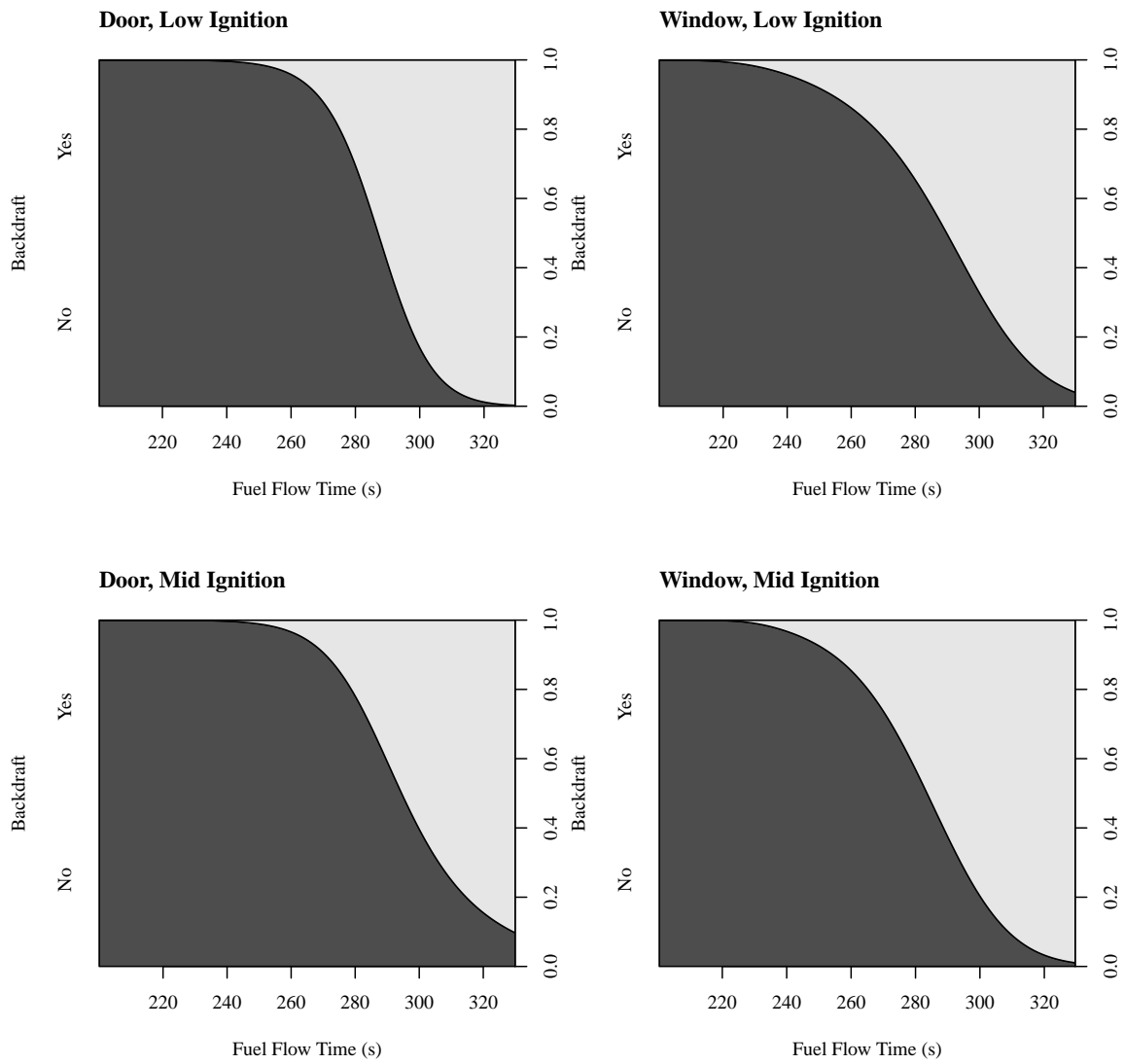
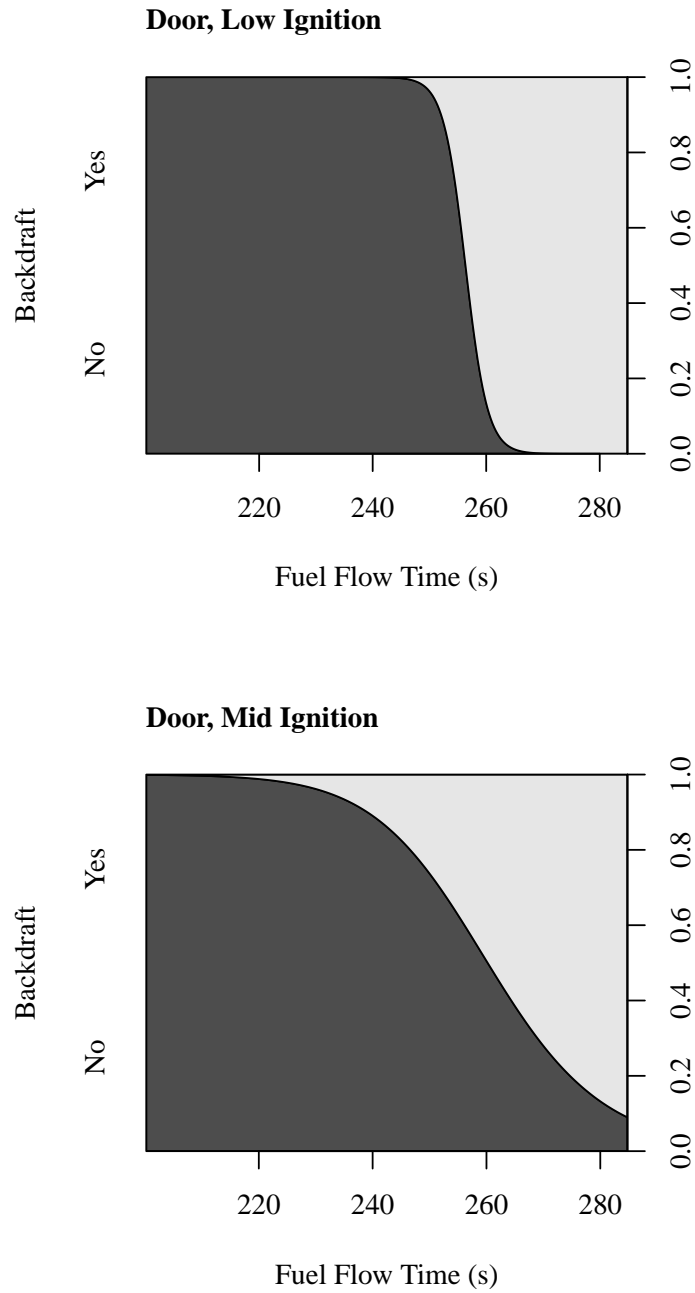
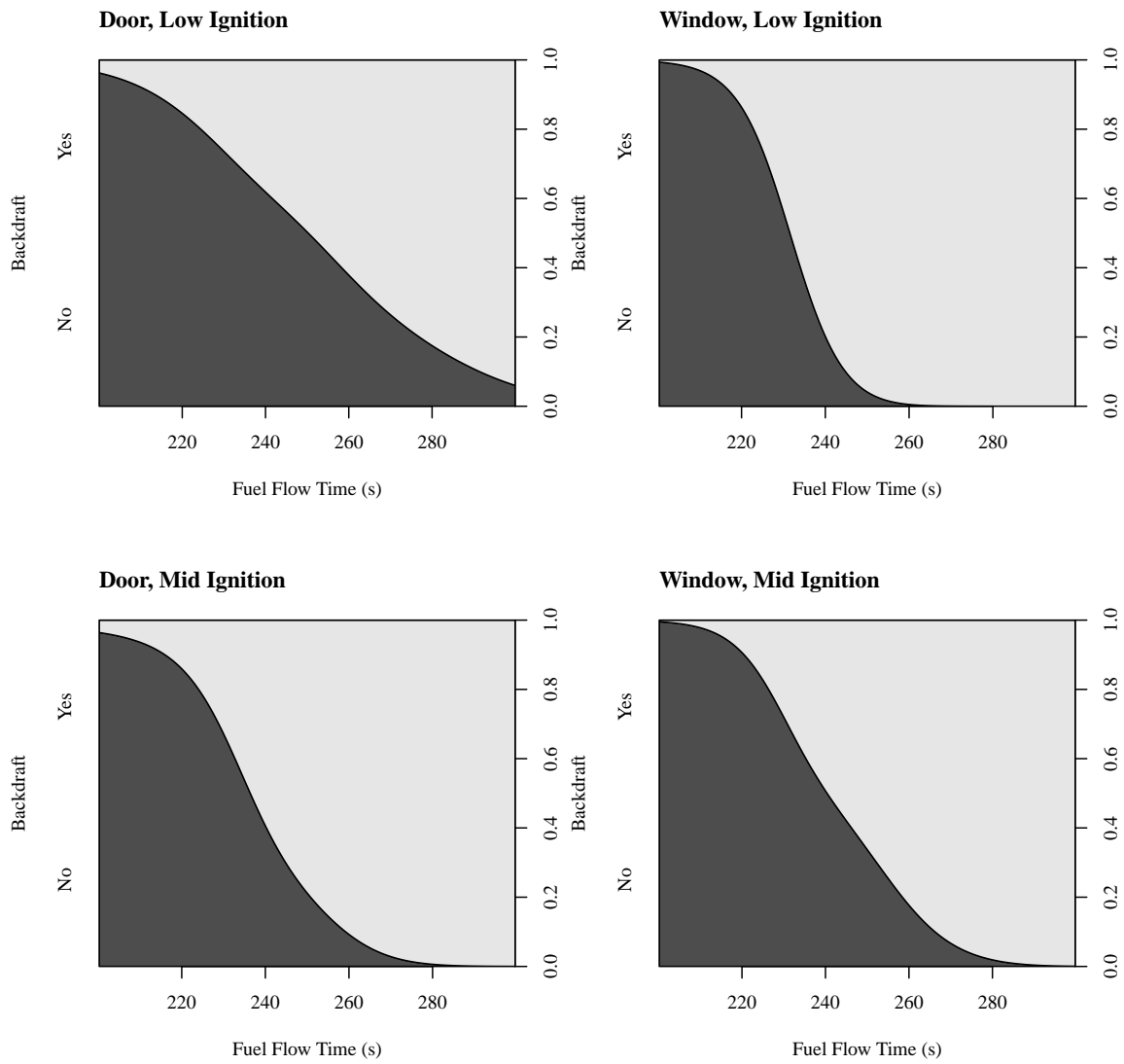


Fig. 22. Conditional density plot of a 16.7 kW propane fire as a function of fuel flow time at various compartment configurations



**Fig. 23.** Conditional density plot of a 20.9 kW propane fire as a function of fuel flow time at various compartment configurations



**Fig. 24.** Conditional density plot of a 25.0 kW propane fire as a function of fuel flow time at various compartment configurations

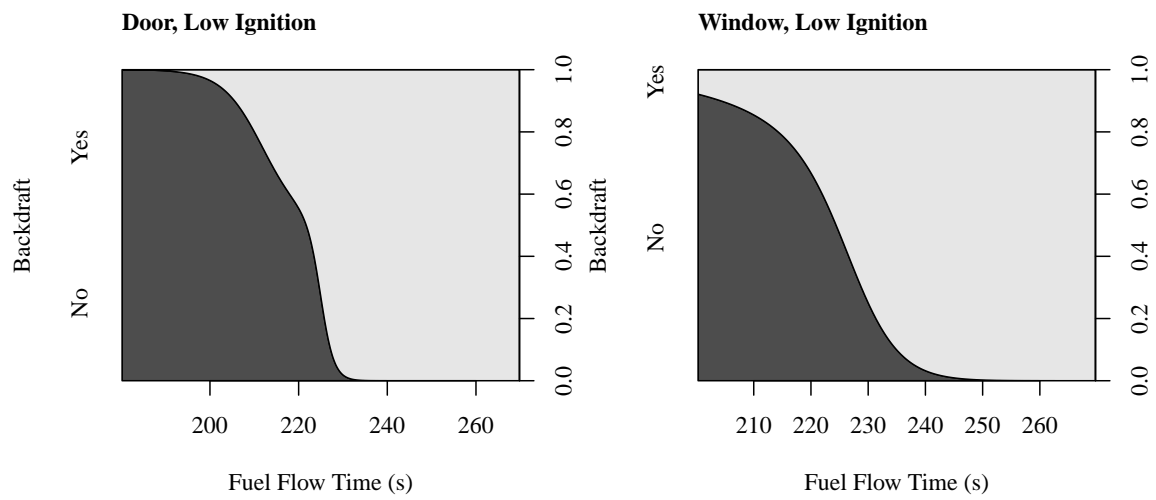


**Fig. 25.** Conditional density plot of a 25.0 kW propylene fire as a function of fuel flow time at various compartment configurations

## 6. Conclusion

In summary, real-time and time-averaged measurements of temperature, global and local equivalence ratios, and O<sub>2</sub>, CO<sub>2</sub>, and CO concentrations on a dry basis are made to characterize conditions prior to an anticipated backdraft in an enclosure subjected to various fuel types, fire sizes, and fuel flow times. In instances where methane was utilized, the gas composition was found to be richer in the upper region of the compartment prior to the doorway opening. For experiments with propane and propylene fires, the fuel settled closer to the bottom of the compartment as fuel flow time increased. Gas mixture composition measurements were verified by GC/MSD, which also provided a detailed description of gas species concentration of extracted gas samples from experiments subjected to different conditions. The likelihood of a backdraft was found to increase with fuel flow rate. A smaller opening and higher spark location were also shown to improve the probability of backdraft.

## References

- [1] Fleischmann C (1993) *Backdraft phenomena*. Ph.D. thesis. University of California, Berkeley, Berkeley, USA.
- [2] Fleischmann C, Pagni P, Williamson R (1994) Quantitative backdraft experiments. *Fire Safety Science-Proceedings of the Fourth International Symposium*, Vol. 4, pp 337–348.
- [3] Fleischmann C, Pagni P, Williamson R (1993) Exploratory backdraft experiments. *Fire Technology* 29(4):298–316.
- [4] Bollinger I (1995) Full residential-scale backdraft Master's thesis University of Canterbury, Christchurch, New Zealand.
- [5] Weng W, Fan W (2003) Critical condition of backdraft in compartment fires: a reduced-scale experimental study. *Journal of Loss Prevention in the Process Industries* 16(1):19–26.
- [6] Weng W, Fan W (2002) Experimental study on the mitigation of backdraft in compartment fires with water mist. *Journal of Fire Sciences* 20(4):259–278.
- [7] Gottuk D, Peatross M, Farley J, Williams F (1999) The development and mitigation of backdraft: a real-scale shipboard study. *Fire Safety Journal* 33(4):261–282.
- [8] Gottuk D, Williams F, Farley J (1997) The development and mitigation of backdrafts: a full-scale experimental study. *Fire Safety Science* 5:935–946.
- [9] Gojkovic D (2000) Initial backdraft experiments (Lund University), 3121.
- [10] Tsai L, Chiu C (2013) Full-scale experimental studies for backdraft using solid materials. *Process Safety and Environmental Protection* 91(3):202–212.
- [11] Chen N (2012) Smoke Explosion in Severally Ventilation Limited Compartment Fires Master's thesis University of Canterbury, Christchurch, New Zealand.
- [12] Parkes A (2009) The Impact of Size and Location of Pool Fires on Compartment Fire Behaviour. Ph.D. thesis. University of Canterbury, Christchurch, New Zealand.
- [13] Park J, Oh C, Choi B, Han Y (2015) Computational visualization of the backdraft development process in a compartment. *Journal of Visualization* 18(1):25–29.
- [14] Ferraris S, Wen J, Dembele S (2008) Large eddy simulation of the backdraft phenomenon. *Fire Safety Journal* 43(3):205–225.
- [15] Weng W, Fan W, Hasemi Y (2005) Prediction of the formation of backdraft in a compartment based on large eddy simulation. *Engineering Computations* 22(4):376–392.
- [16] Park J, Oh C, Han Y, Do K (2017) Computational study of backdraft dynamics and the effects of initial conditions in a compartment. *Journal of Mechanical Science and Technology* 31(2):985–993.
- [17] Horvat A, Sinai Y (2007) Numerical simulation of backdraft phenomena. *Fire Safety Journal* 42(3):200–209.
- [18] Bryant R, Ohlemiller T, Johnsson E, Hamins A, Grove B, Guthrie W, Maranghides A, Mulholland G (2003) The NIST 3 megawatt quantitative heat release rate facility (National Institute of Standards and Technology), NIST Special Publication 1001.

- [19] Cleary T, Falkenstein-Smith R, Brown C (2021) Evolution and characterization of backdraft hazard in a 2/5<sup>th</sup> scale compartment. *Proc. of the 12th Asia-Oceania Symposium on Fire Science and Technology*, Vol. 12, .
- [20] Brown C, Falkenstein-Smith R, Cleary T (2021) Reduced-Scale Compartment Gaseous Fuels Backdraft Experiments (National Institute of Standards and Technology), NIST Technical Note 2183.
- [21] Falkenstein-Smith R, Sung K, Chen J, Harris K, Hamins A (2021) The Structure of Medium-Scale Pool Fires, Second Edition (National Institute of Standards and Technology), NIST Technical Note 2082,e2.
- [22] Falkenstein-Smith R, Harris K, Sung K, Liang T, Hamins A (2022) A calibration and sampling technique for quantifying the chemical structure in fires using gc/msd analysis. *Fire and Materials* 46(1):3–11.
- [23] Babrauskas V, Parker W, Mulholland G, Twilley W (1994) The phi meter: A simple, fuel-independent instrument for monitoring combustion equivalence ratio. *Review of Scientific Instruments* 65(7):2367–2375.
- [24] Falkenstein-Smith R, Cleary T (2021) The Design and Performance of a Second-Generation Phi Meter (National Institute of Standards and Technology), NIST Technical Note 2184.
- [25] Stavropoulos P, Michalakov A, Skevis G, Couris S (2005) Quantitative local equivalence ratio determination in laminar premixed methane–air flames by laser induced breakdown spectroscopy (LIBS). *Chemical Physics Letters* 404(4-6):309–314.
- [26] Han D, Steeper R (2002) An LIF equivalence ratio imaging technique for multicomponent fuels in an ic engine. *Proceedings of the Combustion Institute* 29(1):727–734.
- [27] Hurley M (ed) (2016) *SFPE Handbook of Fire Protection Engineering* (Springer, New York), 5th Ed.

## Appendix A. Uncertainty Analysis of Real-time Measurements

### Appendix A.1. Temperature

The uncertainty of thermocouple measurements is estimated from the Type B evaluation of standard uncertainty determined from the thermocouple error, which is approximately 2.20 °C or 0.75% of the reading, whichever is greater. A coverage factor of 2 is applied to the combined uncertainty to represent a 95 % confidence interval.

### Appendix A.2. Gas Species Concentration Measurements obtained via Gas Analyzer

The uncertainty of individual gas species concentration measurements is estimated from the Type B evaluation of standard uncertainty defined by the bias in the instrumentation. For direct gas analyzer measurements, the uncertainty attributed to the instrument is provided in Table 2. A coverage factor of 2 is applied to the combined uncertainty to represent a 95 % confidence interval.

**Table 2.** List of uncertainties for gas analyzer components.

Components	Manufacturer	Rel. Uncertainty (%)
Paramagnetic O <sub>2</sub> Sensor	California Analytical Instruments, Inc.	2.0
NDIR CO <sub>2</sub> Sensor	California Analytical Instruments, Inc.	4.0
NDIR CO Sensor	California Analytical Instruments, Inc.	4.0

### Appendix A.3. Global Equivalence Ratio

As shown in Eq. 1, real-time measurements of the global equivalence ratio,  $\phi_G$ , is determined from a combination of the volumetric flow reading of the dried exhaust stream,  $\dot{V}_{MFC}$ , the O<sub>2</sub> and CO<sub>2</sub> concentrations within the dried exhaust stream,  $X_{O_2}$  and  $X_{CO_2}$ , and the volumetric flow of excess oxygen introduced in the phi meter's reactor,  $\dot{V}_{O_2,Ex}$ . The uncertainty of the global equivalence ratio is estimated using the law of propagation of uncertainty:

$$u_{\phi_G} = \sqrt{\left(\frac{\partial \phi_G}{\partial \dot{V}_{MFC}} u_{\dot{V}_{MFC}}\right)^2 + \left(\frac{\partial \phi_G}{X_{O_2}} u_{X_{O_2}}\right)^2 + \left(\frac{\partial \phi_G}{\partial X_{CO_2}} u_{X_{CO_2}}\right)^2 + \left(\frac{\partial \phi_G}{\dot{V}_{O_2,Ex}} u_{\dot{V}_{O_2,Ex}}\right)^2} \quad (5)$$

The volume fraction of oxygen in the air,  $X_{O_2,Ent}$ , is included in Eq. 1 and is assumed to be constant and therefore does not affect the global equivalence ratio uncertainty. A coverage factor of 2 is applied to the combined uncertainty to represent a 95 % confidence interval.

The uncertainty of the concentration and flow measurements in Eq. 5 are defined as the Type B evaluation of standard uncertainty, determined from the instrument error provided by the manufacturer. Table 3 lists the instruments incorporated into the phi meter that are used to determine  $\phi_G$ .

**Table 3.** List of uncertainties for selected phi meter components.

Components	Manufacturer	Rel. Uncertainty (%)
High-Temperature Mass Flow Controller	Alicat Scientific, Inc.	0.2
Oxygen Mass Flow Controller	Brooks Instrument	2.0
Mass Flow Meter	Alicat Scientific, Inc.	0.2
Paramagnetic O <sub>2</sub> Sensor	Servomex Group Ltd.	0.5
NDIR CO <sub>2</sub> Sensor	Servomex Group Ltd.	4.0

#### Appendix A.4. Local Equivalence Ratio

Real-time measurements of the local equivalence ratio are calculated via Eq. 2, which incorporates the mass flows of O<sub>2</sub> in the excess oxygen line,  $\dot{m}_{O_2,Ex.}$ , the inlet of the phi meter,  $\dot{m}_{O_2,Samp.}$ , and the outlet of the phi meter's reactor,  $\dot{m}_{O_2,O}$ . The uncertainty of the local equivalence ratio is estimated from the law of propagation of uncertainty:

$$u_{\phi_L} = \sqrt{\left(\frac{\partial \phi_L}{\partial \dot{m}_{O_2,Ex.}} u_{\dot{m}_{O_2,Ex.}}\right)^2 + \left(\frac{\partial \phi_L}{\partial \dot{m}_{O_2,Samp.}} u_{\dot{m}_{O_2,Samp.}}\right)^2 + \left(\frac{\partial \phi_L}{\partial \dot{m}_{O_2,O}} u_{\dot{m}_{O_2,O}}\right)^2} \quad (6)$$

The uncertainty of the oxygen mass flow rates are estimated from the Type B evaluation of standard uncertainty, reported in Ref. [24].

## Appendix B. Uncertainty Analysis of Time-Averaged Measurements

The uncertainty of time-averaged measurements,  $u_{\bar{i}}$  is determined from a combined Type A and B evaluations of standard uncertainty. The Type A evaluation of standard uncertainty of measurements is calculated from the standard error of the averaged readings,  $s_i$ . The Type B evaluation of standard uncertainty of measurements is defined from the bias error sources in the instrumentation,  $u_{\text{inst}}$ . The combined uncertainty of the time-averaged measurements is found via quadrature:

$$u_{\bar{i}} = \sqrt{s_i^2 + u_{\text{inst}}^2} \quad (7)$$